diversity

MDPI

Article

Endocranial Anatomy of the Giant Extinct Australian Mihirung Birds (Aves, Dromornithidae)

Warren D. Handley * and Trevor H. Worthy

Palaeontology Group, Flinders University, GPO 2100, Adelaide 5001, Australia; trevor.worthy@flinders.edu.au
* Correspondence: warren.handley@flinders.edu.au

Abstract: Dromornithids are an extinct group of large flightless birds from the Cenozoic of Australia. Their record extends from the Eocene to the late Pleistocene. Four genera and eight species are currently recognised, with diversity highest in the Miocene. Dromornithids were once considered ratites, but since the discovery of cranial elements, phylogenetic analyses have placed them near the base of the anseriforms or, most recently, resolved them as stem galliforms. In this study, we use morphometric methods to comprehensively describe dromornithid endocranial morphology for the first time, comparing *Ilbandornis woodburnei* and three species of *Dromornis* to one another and to four species of extant basal galloanseres. We reveal that major endocranial reconfiguration was associated with cranial foreshortening in a temporal series along the *Dromornis* lineage. Five key differences are evident between the brain morphology of *Ilbandornis* and *Dromornis*, relating to the medial wulst, the ventral eminence of the caudoventral telencephalon, and morphology of the metencephalon (cerebellum + pons). Additionally, dromornithid brains display distinctive dorsal (rostral position of the wulst), and ventral morphology (form of the maxillomandibular [V_2+V_3], glossopharyngeal [IX], and vagus [X] cranial nerves), supporting hypotheses that dromornithids are more closely related to basal galliforms than anseriforms. Functional interpretations suggest that dromornithids were specialised herbivores that likely possessed well-developed stereoscopic depth perception, were diurnal and targeted a soft browse trophic niche.

Keywords: Cenozoic fossil birds; Galloanserae; dromornithids; brain morphology

Citation: Handley, W.D.; Worthy, T.H. Endocranial Anatomy of the Giant Extinct Australian Mihirung Birds (Aves, Dromornithidae). *Diversity* **2021**, *13*, 124. https://doi.org/10.3390/d13030124

Academic Editor: Eric Buffetaut

Received: 29 January 2021
Accepted: 8 March 2021
Published: 15 March 2021

1. Introduction

The dromornithids were large flightless birds, collectively known as 'mihirungs', whose fossils are a distinctive component of the Cenozoic avifauna of Australia, and are sometimes comparatively abundant in the Australian Neogene fossil record [1,2]. The greatest diversity of the group occurs during the Miocene [1,3–6], but the family is known from fossils dating from the Palaeogene, with a record consisting of a mould of fossil footprints from the Eocene of Queensland [7], postcranial remains from the late Oligocene Pwerte Marnte Marnte Local Fauna (LF) in the Northern Territory [4], and trackways, probably made by dromornithids, reported from the late Oligocene of Tasmania [1,8].

The fossil record shows that the characteristic morphology of dromornithids had already evolved by the late Oligocene, and that it changed little over the next ~20 million years (Ma) until the group became extinct in the late Pleistocene [6,9]. The first dromornithid named was *Dromornis australis* Owen, 1872, from undated deposits at Peak Downs, Queensland [1,6,10–13]. Eight species in four genera of dromornithids are now recognised: Stirling and Zietz [14] named *Genyornis newtoni* Stirling and Zietz, 1896 from Lake Callabonna, South Australia, from what was originally thought to be late Pliocene to early Pleistocene [14] (p. 177), but more recently proposed to be middle to late Pleistocene [15] (p. 16) deposits. Rich [11] described *D. stirtoni* Rich, 1979, *Ilbandornis lawsoni* Rich, 1979 and *I. woodburnei* Rich, 1979 from the late Miocene Waite Formation, Alcoota, Northern Territory, and *Barawertornis tedfordi* Rich, 1979 from the late Oligocene to early Miocene Carl

Creek Limestone at Riversleigh, Northern Queensland. She also named *Bullockornis planei* Rich, 1979 from the middle Miocene Camfield beds, Bullock Creek, Northern Territory [11] (p. 27), but the genus *Bullockornis* was later synonymised with *Dromornis* [12]. This was supported by Worthy et al. [6] upon revision of cranial material of the Bullock Creek specimens, in conjunction with the description of *Dromornis murrayi* Worthy et al., 2016 from Riversleigh. At the same time, Worthy et al. [6] proposed the eight dromornithid species formed two lineages, where the *Dromornis* lineage is monotypic throughout its range, and includes in a temporal succession *D. murrayi*, *D. planei*, *D. stirtoni*, and *D. australis*. The *Ilbandornis/Barawertornis* lineage comprises the more gracile taxa *B. tedfordi*, *I. lawsoni*, *I. woodburnei*, and *G. newtoni*.

Dromornithids were long considered to be ratites [11,14,16–18]. All ratites exhibit reduced wing morphology and are generally large, flightless birds [15,19,20]. These features are shared with dromornithids, but Olson [21] (p. 104) succinctly opined that "large size and flightlessness do not a ratite make", and pointed out that characteristics of the dromornithid mandible, quadrate and pelvis suggested that they were likely derived from an entirely different group of birds. In more recent times, with the discovery of additional cranial elements, phylogenetic analyses by Murray and Megirian [3] concluded that dromornithids were the sister-group of the Anhimidae, and so were Anseriformes. This conclusion was reinforced by Murray and Vickers-Rich [2], who also found similarities to Anseranatidae, a closer sister-group to anatids within Anseriformes. In a phylogenetic study of the affinities of Pelagornithidae (bony-toothed birds), Mayr [22] suggested that dromornithids were likely stem Galloanseres, i.e., a sister group to Galliformes and Anseriformes. A relationship more distant from Anseriformes was also found by Worthy et al. [23], whereby with inclusion of a representative sample of extant galloanseres, representative Neoaves and palaeognaths, and key fossil taxa, *Dromornis* was found to have a stem-galliform relationship. Most recently, Worthy et al. [24,25] used an expanded taxon set, and resolved dromornithids as the sister group to the flightless gastornithids of Eurasia and North America, forming a galloansere clade termed Gastornithiformes Stejneger, 1885. However, the relationship of this clade to either galliforms or anseriforms within Galloanserae, was poorly resolved.

As with gastornithids [26,27], there exists convincing evidence for a herbivorous diet in dromornithids, as some specimens have been preserved with gastroliths [28] (p. 79). Individual stones, presumed to be gastroliths, are common in the fossiliferous silty unit of the Waite Formation producing the Alcoota LF wherein dromornithids are abundant ([2] (p. 262), [29] (p. 164), [30] (Figure 8A)). Undoubted gastroliths in the form of complete or partial gizzard stone sets, are known from several specimens of the Pleistocene dromornithid *Genyornis newtoni*, collected on recent expeditions by THW et al.

Handley et al. [31] demonstrated significant male dominated sexual dimorphism in the largest of all dromornithids, the Miocene species *Dromornis stirtoni*, and revealed those birds identified as male had a mean mass of 528 kg based on tibiotarsus circumference metrics. The tibiotarsus was preferred for estimating body mass in large birds, especially in dromornithids, after statistical evaluations of several mass estimation algorithms applied across a large sample, showed that femoral metrics likely overestimated body mass for them [31,32]. These dromornithids, along with the giant aepyornithid morphotype *Vorombe titan* (Andrews, 1894), from the Holocene of Madagascar [33], likely comprise the largest birds to have ever evolved.

Dromornithid cranial anatomy has previously been comprehensively described [1,3,6], and while Murray and Megirian ([3] (Figure 5)), repeated in Murray and Vickers-Rich ([2] (Figures 78–80)), briefly described a physical endocast for *Dromornis planei*, there exists no information regarding the specific shape and size of the dromornithid brain across the two lineages proposed by Worthy et al. [6].

Worthy et al. [6] identified that from the Oligocene through the late Miocene, the shape of crania of dromornithids changed, with a foreshortening of the length relative to the height of the cranium (e.g., Figure 1). How the shape of the dromornithid brain changed

to accommodate these temporal changes in cranial anatomy and whether there exists quantifiable differences in endocranial anatomy between the *Dromornis* and *Ilbandornis* lineages have yet to be appropriately assessed.

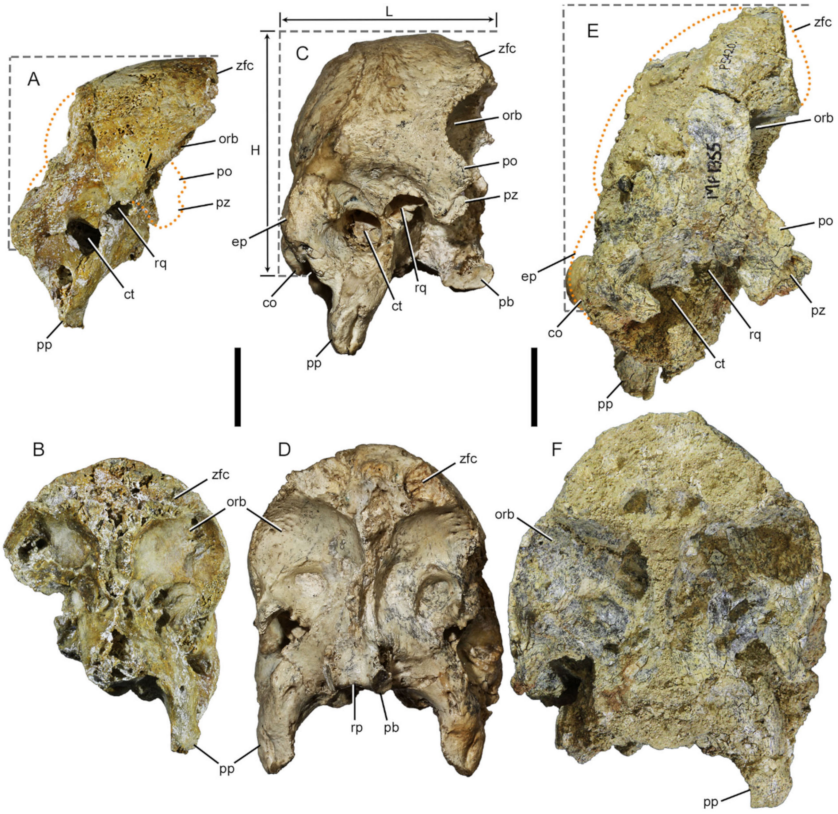

Figure 1. Time series of *Dromornis* specimens showing a progressive increase in cranial height (H) relative to length (L) over ~20–8 Ma: (**A**,**B**), *Dromornis murrayi* (QM F57984) Oligo–Miocene (~25–23 Ma); (**C**,**D**), *D. planei* (NTM P9464-106) middle Miocene (~15–12 Ma); (**E**,**F**), *D. stirtoni* (NTM P5420) late Miocene (~9–7 Ma). Views. Right lateral view (**A**,**C**,**E**); Rostral, (**B**,**D**,**F**). *D. murrayi* lateral view (**A**) shows the more complete left hand side (**B**) which has been flipped for comparison. Missing cranial areas are shown by orange stippled lines on (**A**) and (**E**). Abbreviations: ct, cavum tympanicum; ep, exoccipital prominence; mm, millimetres; orb, orbit; pb, processus basipterygoidei; po, processus postorbitalis; pp, processus paroccipitalis; pz, processus zygomaticus; rp, rostrum parasphenoidalis; rq, recessus quadratica; zfc, zona flexoria craniofacialis. Scale bars equal 40 mm.

The objectives of this study are to assess dromornithid endocast material spanning the late Oligocene to the late Miocene. This will: (1) allow a comprehensive description of morphological characteristics of the dromornithid brain and its principal innervation for the first time; (2) inform our understanding of how dromornithid brains differ morphologically from those of other galloanseres; (3) assess how *Dromornis* and *Ilbandornis* differ in endocranial anatomy; (4) assess how brain shape responded to significant changes in cranial anatomy through time; (5) identify potential functional constraints shaping the evolution of dromornithid endocranial anatomy across this period; and (6) aid in resolving the phylogenetic position of dromornithids.

2. Materials and Methods

2.1. Abbreviations

Institutions

ANSTO, Australian Nuclear Science and Technology Organisation, Lucas Heights, Sydney, New South Wales, Australia, QM, Queensland Museum, Brisbane, Queensland, Australia, QVM, Queen Victoria Museum and Art Gallery, Launceston, Tasmania, Australia;

NTM, Museum of Central Australia, Alice Springs, Northern Territory, Australia, SAHMRI, South Australian Medical and Health Research Institute, Adelaide, South Australia, SAM, South Australian Museum, Adelaide, South Australia, MV, Museums Victoria, Melbourne, Victoria, Australia.

2.2. Geological and Temporal Data for Fossil Specimens

The fossil materials used in this study were sourced from three localities. Two crania of *Dromornis murrayi* (QM F57984; QM F57974), and a fossil endocast (QM F50412) came from Riversleigh World Heritage Area in north-western Queensland, Australia (Figure 1; SI Figures S1–S3). The fossil endocast (QM F50412) was not scanned and does not contribute to numerical analysis, but is figured for comparative purposes (see SI Figure S3). *Dromornis murrayi* (QM F57984) is derived from the Hiatus site (Queensland Museum Locality 941), Hal's Hill, D Site Plateau, forming part of the Riversleigh Faunal Zone A deposits (e.g., "System A" of [34,35] and "Faunal Zone A" of [36,37]). Hiatus site comprises "pure" limestone formed in an aquatic setting, and has proved difficult to successfully date radiometrically, due to the lack of speleothem or flowstone material often included in palaeo-cave deposits elsewhere at Riversleigh [38]. The Hiatus fauna is considered late Oligocene to early Miocene (~25–23 Ma) in age, based on biocorrelation (i.e., vertebrate stage of evolution; see [34–39]). The second specimen of *D. murrayi* (QM F57974), and the fossil endocast (QM F50412), come from Cadbury's Kingdom site, considered Faunal Zone B and early Miocene (~23–16 Ma) in age [37–39].

The second site complex is located at Bullock Creek in the Northern Territory of central Australia: one cranium, respectively, of *Dromornis planei* (NTM P9464-106) and *Ilbandornis woodburnei* (QVM:2000:GFV:20) were studied from this site (Figure 1; SI Figures S4 and S5). The Camfield Beds exposed at Bullock Creek, are fossiliferous freshwater conglomeratic limestone deposits that contain the Bullock Creek LF, which includes several aquatic and "stream-bank" species [30], and forms the type locality for the Camfieldian Land Mammal Age [40]. Fossils from the site are generally well preserved [6], and are considered to be middle Miocene (~14–12 Ma) in age based on biocorrelation, specifically the stage of evolution of diprotodontid *Neohelos* spp. [14,30,38,40,41].

The third site complex is located at Alcoota Station, approximately 110 km north-east of Alice Springs in the Northern Territory of central Australia [42]: two crania of *Dromornis stirtoni* (NTM P5420; NTM P3250) from Alcoota LF were studied (Figure 1; SI Figures S6 and S7). The Alcoota LF derives from unconsolidated fluviatile clays and silts of the Waite formation, previously interpreted as lacustrine deposits [29]. The sediments are now considered to be overbank silts accumulated via debris flow, wherein fossils are concentrated in extensive bonebeds with little or no association [42–45]. Specimens are generally poorly preserved, likely due to repeated fluctuations in moisture content of the siltstone matrix, causing fracturing and compaction of fossils over time [30]. Alcoota LF is believed to be late Miocene (~9–7 Ma) in age based on biocorrelation [1,30,40,44,46], and is the type locality for the Waitean Land Mammal Age [40]. Alcoota LF is unique in that it preserves the only late Miocene vertebrate community known from Australia outside of Riversleigh [2,30].

Four crania of extant basal galloansere birds were also included: the phasianid *Gallus gallus* (SAM B34041), a megapodiid *Leipoa ocellata* (SAM B11482), an anhimid *Anhima cornuta* (MV B12574), and the anseranatid *Anseranas semipalmata* (SAM B48035).

2.3. Nomenclature

We follow the anatomical nomenclature in Baumel et al. [47] for osteology, innervation, and external or brain surface anatomy (see Figure 2, Figure 3A–D, Figure 4A–D; SI Figures S4K–N and S5K–L). Therefore, cranium is the term preferred for that part of the skull enclosing the brain, rather than neurocranium. Descriptions of the internal architecture of the avian brain follow Jarvis et al. [48,49] (Figure 6). At first mention, osteological, innervation, and brain surface anatomy is described using Latin nomenclature, with the

anglicised equivalent in parenthesis, or mentioned immediately subsequent. Thereafter, we use anglicised equivalents where appropriate.

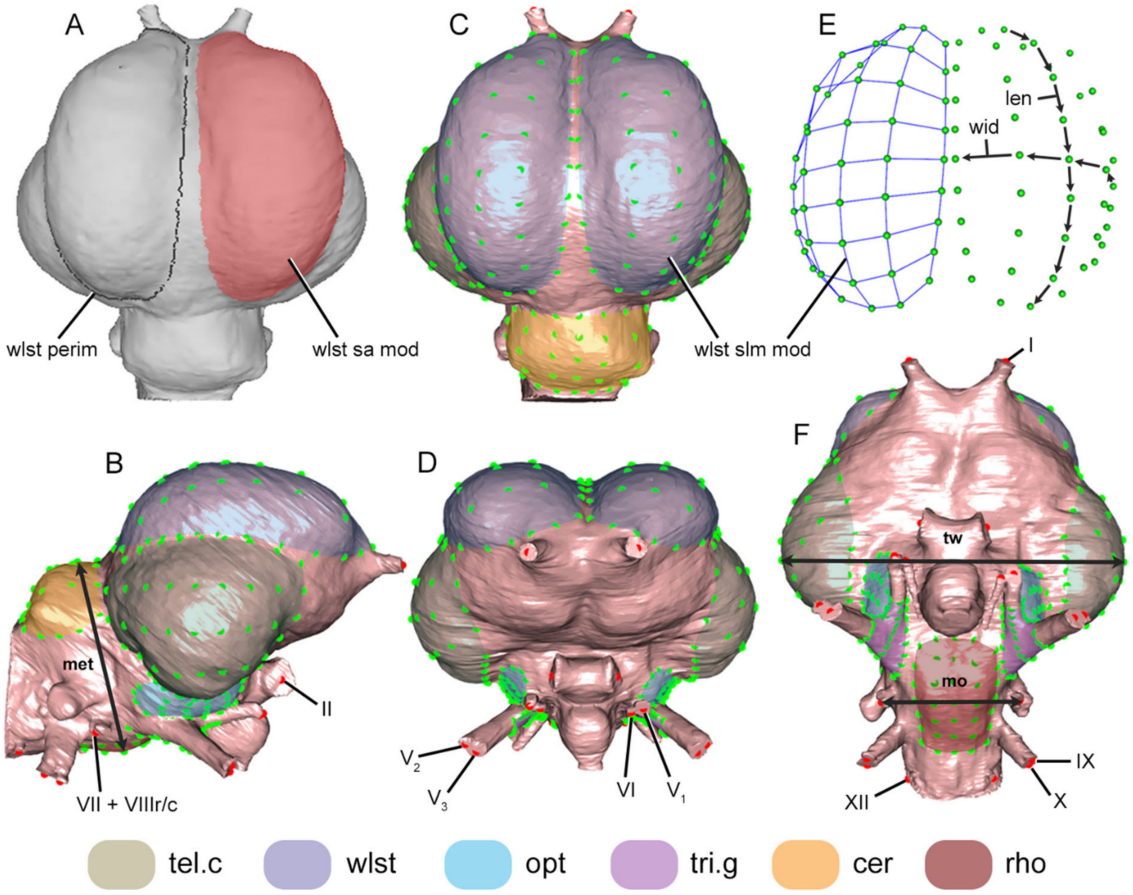

Figure 2. Modular Surface Area (**A**) and Measurement data (**E**), along with landmark modules used to capture endocast shape (see Section 2.6.2, Section 2.6.3 and SI Section S3.2). Brain surface Slm modules (green dots) and innervation Lm module (red dots), are mapped onto the endocast of *Dromornis planei* (NTM P9464-106), and Slm modules are colour-shaded to facilitate anatomical identification (see also SI Figures S10 and S11). Acquisition of Modular Surface Area data are illustrated by a dorsal endocast (**A**), showing the right side wulst surface area module selected (wlst sa mod–pink), prior to computation of the surface area value for the defined region. The endocast (**A**) also shows the previously defined left side wulst module, circumscribed by a perimeter polyline (wlst perim) for which the surface area value was computed (see Section 2.6.3 above). Measurement values are illustrated by a 3D shape plot (**E**) showing wulst Slm modules (wlst slm mod), left side Slms (green dots) are linked (blue) to provide perspective. Distance (vector) values were calculated between individual Slms forming the modular width (**wid**) and length (**len**) measurements, vector values were then combined to form the total measurement value; Measurements were also calculated between individual Slms for; (**met**), metencephalon (cerebellum + pons) total height; (**tw**), endocast total width; (**mo**), medulla oblongata total width (see Section 2.6.2 above). Views: (**A**,**C**,**E**), Dorsal; (**B**), right lateral; (**D**), rostral; (**F**), ventral. Abbreviations: cer, cerebellum; Lm, landmark; mod, module; opt, optic lobe; perim, perimeter; rho, rhombencephalon; sa, surface area; Slm, semilandmark; tel.c, caudal telencephalon; tri.g, trigeminal ganglion; wlst, wulst; I, left olfactory nerve; II, right optic nerve; V_1, ophthalmic nerve; V_2, maxillary nerve; V_3, mandibular nerve; VI, abducent nerve; VII + VIIIr/c, rami of the facial nerve (VII), and the rostral (VIIIr) and caudal (VIIIc) vestibulocochlear nerves; IX, glossopharyngeal nerve; X, vagus nerve; XII, ramus of the hypoglossal (XII) nerve (XIIc in the extant galloanseres (Section 3.1.6, Figure 4D; SI Figures S10C and S11C). Endocasts are not to scale. [Note: for the modular Slm suite mapped onto the endocast of *Leipoa ocellata* (MV B12574), see SI Figures S10 and S11).

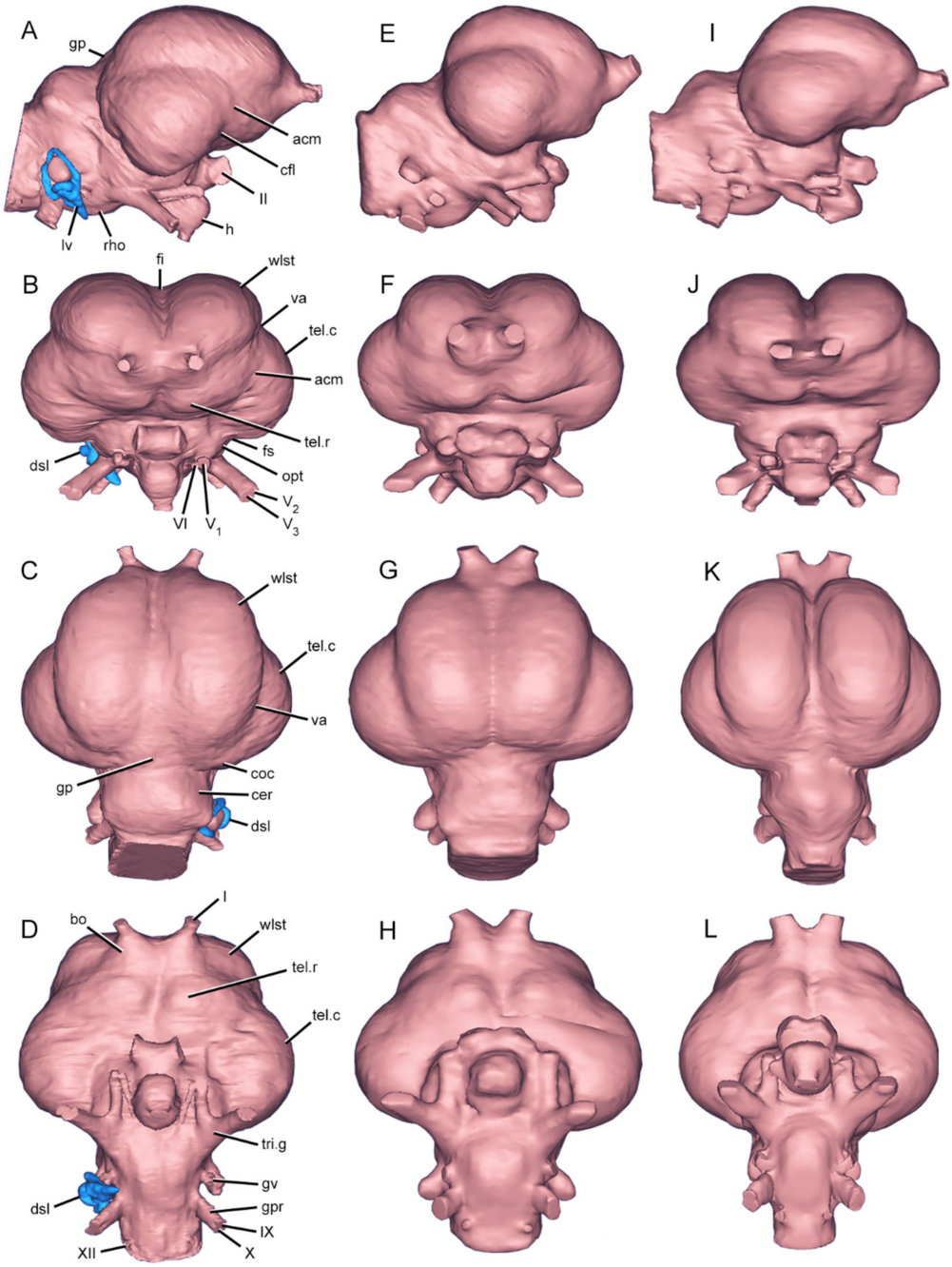

Figure 3. Dromornithid endocasts: (**A**–**D**), *Dromornis planei* (NTM P9464-106); (**E**–**H**), *D. murrayi* reconstruction (QM F57984 + QM F57974; see SI Figure S9); (**I**–**L**), *Ilbandornis woodburnei* (QVM:2000:GFV:20). Views. Right lateral (**A**,**E**,**I**); rostral (**B**,**F**,**J**); dorsal (**C**,**G**,**K**); ventral (**D**,**H**,**L**). Trigeminal nerves (V_1, V_2, V_3) are truncated where exiting the cranium. Abbreviations: acm, arteria cerebralis medialis; bo, olfactory bulb; cer, cerebellum; cfl, cerebrum fovea limbica; coc, cerebrum pars occipitalis; dsl, lateral semicircular duct; fi, fissura interhemispherica; fs, fissura subhemispherica; gp, glandula pinealis; gpr, proximal ganglion; gv vestibular ganglion; h, hypophysis; lv, vestibular organ (semicircular ducts + cochlea [blue]; see also Section 4.1.4); mm, millimetres; opt, optic lobe; rho, rhombencephalon; tel.c, caudal telencephalon; tel.r, rostral telencephalon; tri.g, trigeminal ganglion; va, vallecula telencephali; wlst, wulst; I, olfactory nerve; II, optic nerve; V_1, ophthalmic nerve; V_2, maxillary nerve; V_3, mandibular nerve; VI, abducent nerve; IX, glossopharyngeal nerve; X; vagus nerve; XII, ramus of the hypoglossal nerve. Endocasts are not to scale.

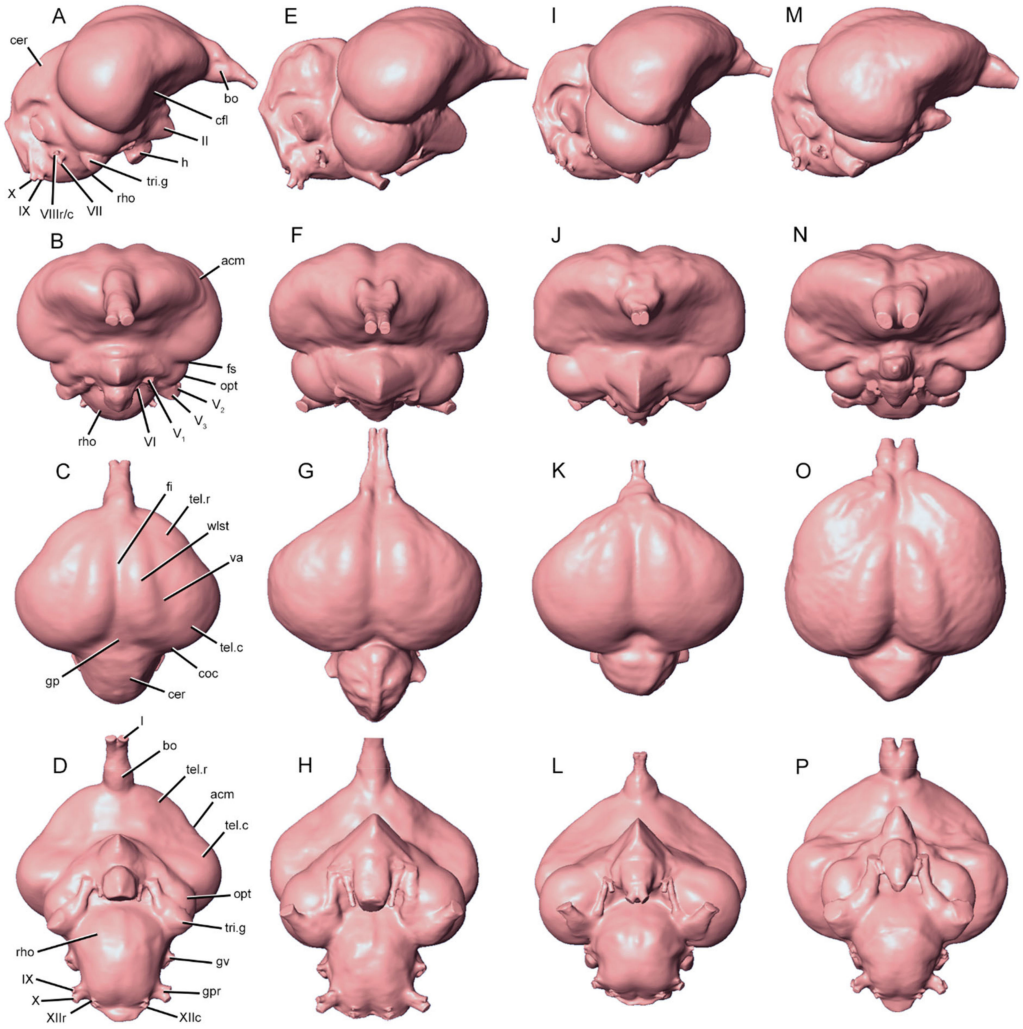

Figure 4. Galloansere endocasts. (**A**–**D**), *Anhima cornuta* (MV B12574); (**E**–**H**), *Gallus gallus* (SAM B34041); (**I**–**L**), *Leipoa ocellata* (SAM B11482); and (**M**–**P**), *Anseranas semipalmata* (SAM B48035). Views: Right lateral (**A**,**E**,**I**,**M**); Rostral (**B**,**F**,**J**,**N**); Dorsal (**C**,**G**,**K**,**O**); Ventral (**D**,**H**,**L**,**P**). The full extension of the olfactory (**I**) nerves in *G. gallus* are shown in dorsal (**G**) view, but were cropped in lateral (**E**) and ventral (**H**) views to fit the plate. Abbreviations: acm, arteria cerebralis medialis; bo, olfactory bulb; cer, cerebellum; cfl, cerebrum fovea limbica; coc, cerebrum pars occipitalis; fi, fissura interhemispherica; fs, fissura subhemispherica; gp, glandula pinealis; gpr, proximal ganglion; gv vestibular ganglion; h, hypophysis (note the caudoventral hypophysis has been trimmed to facilitate access to rostroventral rhombencephalon surfaces); opt, optic lobe; rho, rhombencephalon; tel.c, caudal telencephalon; tel.r, rostral telencephalon; tri.g, trigeminal ganglion; va, vallecula telencephali; wlst, wulst; I, olfactory nerve; II, optic nerve; V_1, ophthalmic nerve; V_2, maxillary nerve; V_3, mandibular nerve; VI, abducent nerve; VII, facial nerve; VIIIr/c, rostral and caudal rami of the vestibulocochlear nerve; XIIr, rostral and; XIIc, caudal rami of the hypoglossal nerve. Endocasts are not to scale.

Much disparate terminology has been used for the description of surface morphology of the avian cranium and brain, and in some instances with no consensus for precedence of any particular term over another (e.g., see [47,48], and references therein). We agree with Early et al. [50] who considered the term 'wulst' (wlst, Figure 2, Figure 3B–D and Figure 4C) appropriate to describe the external dorsal eminences of the internal hyperpallium [49] (Figure 6), and lobus opticus (optic lobe; opt, Figures 2, 3B and 4B,D) to describe the external ventral eminences of the internal tectum opticus (optic tectum), or tectum mesencephali (mesencephalon). Additionally, we use cerebrum pars frontalis (rostral telencephalon; tel.r, Figure 3B,D and Figure 4C,D; see also Section 2.5), to describe the surface topology of dorsorostrolateral mesopallium and nidopallium [49] (Figure 6), rostrad of the arteria cerebralis medialis (medial cerebral artery; acm, Figure 3A–B and Figure 4B,D) dorsoventral

traversal of the hemispherium telencephali (telencephalic hemisphere); cerebrum pars parietalis (caudal telencephalon; tel.c, Figure 2, Figure 3B–D and Figure 4C–D), to describe the surface topology of the mesopallium, nidopallium and arcopallium [49] (Figure 6), forming part of the caudolateral telencephalon pallial complex caudad of the traversal of the medial cerebral artery (see Section 2.5 below); ganglion trigeminale (trigeminal ganglia, tri.g, Figures 2, 3D and 4A,D) to describe ganglia of the trigeminal nerve (V) complex (see Section 3.1.3 below), inserting on the ventral surface of the optic lobe.

2.4. Modelling

One cranium each of the following species were micro-computed tomography (μCT) scanned using the Skyscan 1076 μCT instrument (Bruker microCT) at Adelaide Microscopy, University of Adelaide: *Gallus gallus*, 17.0 micrometre (μm) resolution, at 59 kilovolts (kV) and 167 microamps (μA); *Leipoa ocellata*, 17.4 μm resolution, at 48 kV and 139 μA; *Anhima cornuta*, 34 μm resolution, at 100 kV and 100 μA; and *Anseranas semipalmata*, 34.8 μm resolution, at 100 kV and 90 μA. Skyscan μCT acquisition data were reconstructed using NRecon v1.6.10.4 (Bruker microCT) and compressed using ImageJ v1.51w [51] software.

The crania of *D. murrayi*, *D. stirtoni* and *I. woodburnei* were medical X-ray CT scanned using the Siemens Somatom Force CT instrument located at the SAHMRI facility in Adelaide. Acquisition CT data were captured at a slice thickness of 0.4 mm, but with the application of an oversampling technique allowing the acquisition of twice the number of slices per detector row, an effective resolution of 240 μm was achieved for all specimens, excluding *D. stirtoni* (NTM P3250) which was CT scanned at a resolution of 320 μm. Acquisition data were reconstructed by M. Korlaet of Dr Jones and Partners using Siemens proprietary software.

The cranium of *D. planei* was scanned at the ANSTO nuclear facilities in Sydney using the DINGO neutron CT instrument, located in the OPAL reactor beam hall on thermal beam HB2. Neutron CT acquisition data were captured at low-intensity mode at 95 μm resolution and were reconstructed by Dr. J. Bevitt of ANSTO. All CT data used were isotropic.

2.4.1. Three-Dimensional (3D) Surface Model Construction

Three-dimensional (3D) surface model construction was conducted via segmentation using Materialise Mimics v18 software, and 3D surface stereolithograph (STL) endocast models were produced from reconstructed CT data to represent the shape of the brain (Figures 3 and 4). These included the base and immediate stem of the major nerves passing from the cranium into the brain (see also Section 3.1, Section 4.4.1 and SI Section S3.1.1). Surface STL models were exported to Materialise Mimics 3-Matic v10 software for reconstruction and remeshing.

2.4.2. Model Reconstructions

In many fossils, structures are often lost or damaged by taphonomic processes over time, or during recovery. Where specimens are somewhat bilaterally symmetrical, as is the case of endocasts, damaged or missing structures may be digitally reconstructed based on preservation of one side, or parts of a particular endocast. The incomplete endocasts for the two fossil specimens of *D. stirtoni* NTM P5420 and NTM P3250 constrained their interpretation. Thus, a two-dimensional (2D) reconstruction representative of the species was derived using both endocast models (see SI Figure S8 and Section S2.1). Similarly, endocasts for specimens of *D. murrayi* were, respectively, damaged and incomplete, where QM F57984 preserves only the left hand side (LHS) dorsolateral endocast, and QM F57974 preserves only the ventral endocast. Consequently, a single 3D endocast model was compiled from CT data of the two specimens of *D. murrayi* (see SI Figure S9 and Section S2.2).

2.4.3. Remeshing

Remeshing of 3D STL surface models is required to optimise the quality of the triangles comprising the surface mesh, and to reduce the file size of models for landmarking

(see below). Remeshing operations were carried out in Materialise 3-Matic v10 and passing of remeshed STL objects to Polygon File Format (PLY) was conducted in MeshLab v2016.12 [52].

2.5. Landmarking

To capture the shape of the endocasts, we defined seven morphological zones using semilandmark (Slm) patches, or modules (see Figure 2; SI Figures S10 and S11, Section S3.2). This approach allowed us to assess whether each morphological zone differed in the same way between taxa and along a lineage, or whether the zones differed in contrasting ways across specimens.

Additionally, the dorsal endocast of dromornithids is dominated by wulst structures (e.g., Figures 2 and 3), which are distinct with respect to those of the extant galloanseres (e.g., wlst, Figure 3 versus [vs] Figure 4, and Section 3.2.2 below). We prefer the explanation that the expansion, or hypertrophy, of the wulst in dromornithids has effectively masked the surface morphology of the rostrodorsal telencephalon (see Section 3.2.1 below). This required the segregation of telencephalic hemispheres into rostral and caudal regions, defined by the traversal of the medial cerebral artery (see acm, Figure 4B, and SI Sections S3.2.1.3–S3.2.1.5), such that telencephalic regions caudal of the medial cerebral artery might be compared across all specimens.

Digital landmarking of 3D endocast surface models was conducted in IDAV Landmark v3.6 [53] using 20 fixed (type 1) and 460 semi- (type 3) landmarks [54] for a total of 480. The set of landmarks (Lms) and semilandmarks (Slms) comprising the modules (Figure 2; SI Figures S10 and S11) were the basis for all subsequent shape assessment. Endocast landmarking protocols and descriptions of the full Modular landmark (Lm) suite are given in Supplementary Information (SI, Section S3).

2.6. Data

We used Slm modules to capture the shape of discrete regions of the brain (see Section 2.5 above). Derived from those shape data (see Section 2.6.1), we computed Measurement data (see Section 2.6.2), and acquired Surface Area data based on the 'footprint' of Slm modules as defined (see Section 2.6.3), with the exception of trigeminal ganglion data, where Measurement data were computed from trigeminal ganglia Slm modules (e.g., Figure 10C and Figure 11C), and Surface Area data were computed from the truncated faces of the maxillomandibular (V_2+V_3; see Figure 2E, Figure 3B and SI Figure S5L) branch of the trigeminal (V) nerve complex (see Figures 3D and 4A,D). Collectively, those three forms of data informed the systematic assessment of morphological differences between the endocasts of individual dromornithid specimens (see Section 2.7.2, Section 3.3 and SI Section S4), and the comparison of dromornithid endocast morphology with those of the extant galloanseres (see Section 3.4 and SI Section S5).

2.6.1. Modular Lm Data

Three-dimensional digital shape data derived from the Modular Lm suite (Figure 2; SI Figures S3, S10 and S11) were used for all assessments of shape (see Section 2.7 below).

2.6.2. Measurement Data

Measurement data were calculated between Lm and Slm locations along specific transects for each specimen, using the 'interlmkdist' function in Geomorph v3.1.3 [55]; see also Section 2.7 below. Measurements for the length and width of each modular structure, capturing the directional 'curve' over a 3D surface, were calculated by adding together the distances between each Slm forming the measurement vector (see Figure 2E). Data for each paired structure (i.e., wulst, rostral and caudal telencephalon, optic lobe, and trigeminal ganglion modules) were combined, and mean Measurement values calculated (see Table 1A). Additionally, measurements describing gross endocast morphological 'vector' distances were calculated between two Lm or Slm locations (see Figure 2B,F;

Table 1A). Size-standardised mean Measurement log shape ratios were calculated by the log shape ratios method [56], where species Measurement values were divided by species endocast total volume values and $\log_{10}$ transformed [57] (p. 99), [58] (p. 117). The log shape ratio approach produces size-standardised shape variables from univariate data and is analogous with the Procrustes superimposition method for multivariate Lm data (i.e., GPA; see Section 2.7.1 below), where both methods correct for size while retaining shape variation [59] (p. 1389). Measurement log shape ratios are presented in text, in Table 1B, and plotted in SI Figures S12 and S13.

Table 1. **A**, Mean Measurement values calculated between Slm locations for each species. **B** and **D**, respectively, Size-standardised Mean Measurement and modular Surface Area log shape ratios. Log shape ratios were calculated by the log shape method (see Section 2.6.2). **C**, Mean modular Surface Areas computed directly from endocast surfaces (see Section 2.6.3). All bilateral structure data (i.e., wulst, rostral and caudal telencephalon, optic lobe, and trigeminal ganglion modules) were combined and mean values calculated. Abbreviations: *A. cornuta*, *Anhima cornuta* (MV B12574); *A. semipalmata*, *Anseranas semipalmata* (SAM B48035); Cer, cerebellum; *D. murrayi*, *Dromornis murrayi* reconstruction (QM F57984 + QM F57974); *D. planei*, *Dromornis planei* (NTM P9464-106); Endo Surf, endocast total surface area; Endo Vol, endocast total volume; *G. gallus*, *Gallus gallus* (SAM B34041); *I. woodburnei*, *Ilbandornis woodburnei* (QVM:2000:GFV:20); L, length; *L. ocellata, Leipoa ocellata* (SAM B11482); Med.Ob, medulla oblongata; Meten, metencephalon; mm, millimetres; mm^2, square millimetres; mm^3, cubic millimetres; Opt, optic lobe; Rho, rhombencephalon; Slm, semilandmark; Tel.c, caudal telencephalon; Tel.r, rostral telencephalon; TH, total height; Tri.g F, trigeminal ganglion maxillomandibular (V_2 + V_3) face; TW, total width; W, width; Wlst, wulst.

Measurement	A. Mean Measurement Values (mm)						
	G. gallus	*L. ocellata*	*A. cornuta*	*A. semipalmata*	*D. murrayi*	*D. planei*	*I. woodburnei*
Wlst L	12.47	14.32	16.79	20.50	55.90	67.65	51.32
Wlst W	4.81	5.52	6.34	7.92	27.63	34.43	28.87
Tel.r L	5.59	9.59	10.37	17.73	N/A	N/A	N/A
Tel.r W	4.02	5.45	8.13	11.93	N/A	N/A	N/A
Tel.c L	15.46	12.75	17.30	17.52	47.26	49.71	41.88
Tel.c W	12.91	13.40	18.43	22.18	41.14	40.61	30.52
Opt L	15.08	18.25	13.37	15.87	16.96	19.11	16.72
Opt W	5.98	7.81	4.67	4.85	6.75	5.96	8.02
Tri.g L	5.96	4.32	7.95	9.60	13.47	13.76	12.30
Tri.g W	4.83	3.76	3.03	3.32	9.56	9.20	9.18
Cer L	12.73	10.95	17.53	15.27	17.79	20.85	21.24
Cer W	10.71	9.91	13.63	17.55	37.87	45.99	33.21
Rho L	9.69	10.71	13.64	14.54	25.65	26.82	23.47
Rho W	7.66	9.51	12.39	10.03	18.19	18.02	13.83
Tel.c TW	21.07	22.25	28.21	31.16	67.34	72.83	57.52
Meten TH	15.43	16.26	20.34	22.04	38.85	40.68	34.56
Med.Ob TW	12.94	11.66	14.33	15.50	37.87	40.59	28.91
Endo Vol (mm^3)	3733.84	4519.27	8031.85	10881.35	95577.71	122859.93	60289.34
	B. Mean Measurement Log Shape Ratios						
Wlst L	0.127	0.163	0.157	0.186	0.362	0.415	0.368
Wlst W	−0.287	−0.251	−0.266	−0.227	0.056	0.122	0.119
Tel.r L	−0.221	−0.011	−0.052	0.123	NA	NA	NA
Tel.r W	−0.365	−0.257	−0.158	−0.049	NA	NA	NA
Tel.c L	0.220	0.113	0.170	0.118	0.289	0.281	0.280
Tel.c W	0.142	0.134	0.198	0.220	0.229	0.193	0.143
Opt L	0.210	0.268	0.058	0.075	−0.156	−0.134	−0.119
Opt W	−0.193	−0.101	−0.398	−0.440	−0.556	−0.640	−0.438
Tri.g L	−0.194	−0.358	−0.167	−0.143	−0.256	−0.276	−0.252
Tri.g W	−0.285	−0.418	−0.587	−0.604	−0.405	−0.452	−0.379
Cer L	0.136	0.046	0.176	0.058	−0.135	−0.096	−0.015
Cer W	0.061	0.003	0.067	0.119	0.193	0.248	0.180
Rho L	0.017	0.037	0.067	0.037	0.024	0.013	0.029
Rho W	−0.085	−0.015	0.025	−0.124	−0.125	−0.159	−0.201
Tel.c TW	0.355	0.354	0.382	0.368	0.443	0.447	0.418
Meten TH	0.219	0.218	0.240	0.218	0.204	0.194	0.197
Med.Ob TW	0.143	0.074	0.088	0.065	0.193	0.193	0.119

Table 1. *Cont.*

Measurement	A. Mean Measurement Values (mm)						
	G. gallus	***L. ocellata***	***A. cornuta***	***A. semipalmata***	***D. murrayi***	***D. planei***	***I. woodburnei***
Module	**C. Mean modular Surface Area Values (mm^2)**						
Wlst	58.50	65.71	90.65	117.40	1353.96	1851.49	1170.99
Tel.r	19.62	47.39	82.55	216.04	NA	NA	NA
Tel.c	144.52	133.10	249.41	297.48	1213.28	1297.48	852.94
Opt	78.90	118.28	52.33	71.57	139.37	164.03	145.83
Tri.g F	1.342	1.335	5.114	6.237	14.537	13.477	10.431
Cer	124.10	103.59	205.25	192.07	678.37	816.82	528.19
Rho	63.21	86.91	136.69	135.38	394.24	585.79	290.76
Endo Surf (mm^2)	1544.33	1682.29	2404.61	2985.52	13199.82	15874.02	10200.52
	D. Mean Modular Surface Area Log Shape Ratios						
Wlst	0.176	0.136	0.079	0.078	0.655	0.720	0.708
Tel.r	−0.299	−0.006	0.039	0.343	NA	NA	NA
Tel.c	0.569	0.443	0.519	0.482	0.608	0.566	0.571
Opt	0.306	0.391	−0.159	−0.137	−0.332	−0.332	−0.196
Tri.g F	−1.464	−1.556	−1.169	−1.197	−1.314	−1.418	−1.342
Cer	0.502	0.334	0.434	0.292	0.355	0.365	0.363
Rho	0.210	0.258	0.258	0.140	0.119	0.221	0.103

2.6.3. Surface Area Data

Surface Area data for each endocast module as defined here (see SI Section S3.2) were computed directly from the surface of each endocast using MeshLab v2016.12 (see Figure 2A). Two forms of Surface Area data were acquired: (1) total endocast Surface Area; and (2) modular Surface Area in square millimetres (mm^2), from which mean Surface Area values for all bilateral modules (i.e., wulst, rostral and caudal telencephalon, optic lobe, and trigeminal ganglion face) were computed (see Table 1C). Size-standardised mean Surface Area log shape ratios were calculated by the log shape ratios method, where species Mean Surface Area values were divided by species endocast Surface Area values and $\log_{10}$ transformed (see Section 2.6.2 above). Surface Area log shape ratios are presented text, in Table 1D, and plotted in SI Figure S14.

Additionally, due to taphonomic processes over some 14 Ma, the caudoventral endocast of *Dromornis planei* had suffered somewhat of a rostrocaudal ventral rotation, along with a subtle rostrally orientated 'twisting' of the caudoventral endocast with respect to dorsal endocast surfaces. This can be appreciated in the slight caudal displacement of LHS optic lobe margins in the *D. planei* endocast, when observed from the ventral aspect (see Figures 2F and 3D below), and in the *D. planei* cranium itself (see Figure 1D above). During landmarking, optic lobe and trigeminal ganglion module margins on the ventral *D. planei* endocast were situated with respect to existing morphological boundaries (see SI Section S3.2.1.9), without attempting to adjust margins for the subtle taphonomic distortion present in the endocast. Subsequent univariate Measurement and Surface Area data for the optic lobe and trigeminal ganglia formed the primary focus for downstream morphological assessments, as the computation of mean log shape ratio values from those paired modular data (see Section 2.6.2 above), accommodated for the subtle bilateral misalignment of ventral midbrain regions in the *D. planei* endocast.

2.7. Analyses

All data analyses and visualisations (Figure 2, Figure 5 and SI Figure S15), excluding SI Figures S12–S14 (OriginPro v2018b.95.1.195, OriginLab Corporation), were conducted in R v3.6.1 [60] using RStudio v1.2.5019 [61], and package Geomorph v3.1.3.

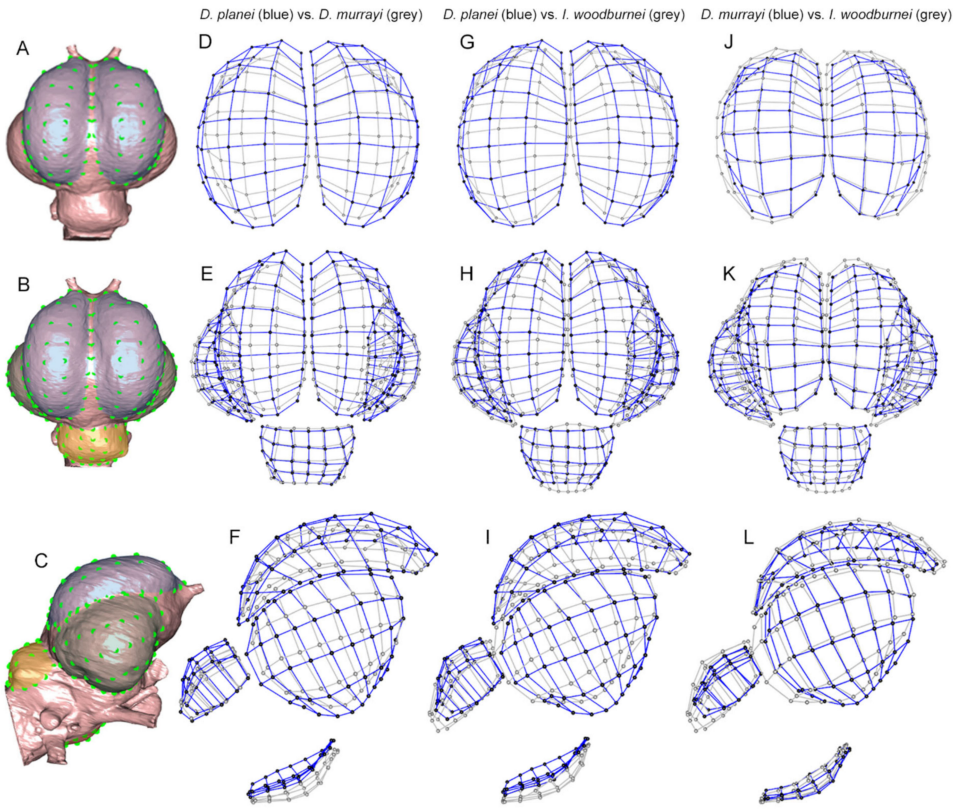

Figure 5. Three-dimensional modular shape variation plots for dromornithid specimens (see Section 2.7.2). (**A**), *Dromornis planei* (NTM P9464-106) endocast showing the caudodorsal view of the wulst (grey) Slm modules represented in plots (**D**), (**G**), and (**J**); (**B**), *D. planei* (NTM P9464-106) endocast showing the dorsal view of the wulst (grey), caudal telencephalon (green) and cerebellum (yellow) Slm modules represented in plots (**E**,**H**,**K**); (**C**), *D. planei* (NTM P9464-106) endocast showing the right lateral view of the wulst (grey), caudal telencephalon (green), cerebellum (yellow), and rhombencephalon (brown) Slm modules represented in plots (**F**,**I**,**L**). Modular Slms (green dots) are mapped onto the inset endocasts, and modules are colour-shaded to assist identification (see Figure 2; SI Figures S10 and S11). Shape variation plots are arranged by column (see column header): (**D**–**F**), *D. planei* (NTM P9464-106–blue) vs. *D. murrayi* reconstruction (QM F57984 + QM F57974–grey); (**G**–**I**), *D. planei* (NTM P9464-106–blue) vs. *Ilbandornis woodburnei* (QVM:2000:GFV:20–grey); (**J**–**L**), *D. murrayi* reconstruction (QM F57984 + QM F57974–blue) vs. *I. woodburnei* (QVM:2000:GFV:20–grey). Abbreviations: Slm, semilandmark; vs., versus.

2.7.1. Generalized Procrustes Analysis (GPA)

Generalized Procrustes Analysis [62,63] is how shape variables, or Procrustes coordinates, are derived from specimen landmark data which are translated, scaled, and optimally rotated using a least-squares criterion [64,65]. During superimposition, Slms on curves and surfaces were slid along tangent directions and tangent planes, respectively [66–69], and locations of Slms were optimised by minimising bending energy [66,67]. Aligned Procrustes coordinates were used for subsequent assessments of shape differences between specimens. The advantage of this approach allows for specimen data to be translated, scaled, and rotated about a common centroid, and shape differences between specimens may be examined within a shared shape space (see below).

2.7.2. Three-Dimensional Modular Shape Variation Plots

To better understand the extent of particular morphological variation between species of dromornithid, we used 3D shape variation plots to visualise the modular shape variation between individual specimens. One dromornithid species represented by black dots and blue links, is superimposed over another represented by grey dots and grey links, visualising the extent and direction of modular shape variation between the two specimens. In this manner, the morphological differences between the endocasts of each species of dromornithid were described (see Figure 5, Section 3.3 and SI Section S4).

3. Results

3.1. Dromornithid Innervation That Differs from the Extant Galloanseres (see Figures 3 and 4; SI Figures S4 and S5)

3.1.1. Nervus Olfactorius

The olfactory (I) nerve transmits rostrocaudally into the bulbus olfactorius (olfactory bulb; bo, Figures 3D and 4D), through the bony foramen n. olfactorii (folf, SI Figures S4K–S4L, S5K) of the rostrodorsal cranium. The dromornithid olfactory bulb is best described by the more complete RHS lateral view of *D. murrayi* (Figure 3E). The margins of the olfactory bulb are pronounced both dorsally and ventrally, but caudodorsally masked by the rostral eminence of the wulst. The caudomediolateral transmission of the olfactory bulb margins are shown by the ventral view of *D. murrayi* and *D. planei* (Figure 3D,H, respectively) as transitioning into the rostroventral endocast without reduction in mediolateral width, as seen most notably in *A. cornuta* and *A. semipalmata* (e.g., Figure 4C,D,O,P, respectively).

3.1.2. Nervus Opticus

The optic (II) nerves form the chiasma opticum caudally, and pass through the os laterosphenoidale, forming the caudomedial wall of the orbit via the foramen opticum (fopt, SI Figures S4K,L and S5K), meeting rostrally at the septum interorbitale. In dromornithids, the interorbital septum rostral of the foramen opticum is robust, and the optic (II) nerves divides rostrolaterally into two well defined branches (i.e., II; Figures 3A and 4A).

3.1.3. Nervus Trigeminus

The trigeminal (V) nerve complex comprises three divisions. The medial or ophthalmic branch carries nervus ophthalmicus (ophthalmic [V_1] nerve; Figures 3B and 4B), transmitting to the trigeminal ganglia (see Section 3.2.5 below) on the ventral surfaces of the optic lobe (see Section 3.2.4 below), through the foramen n. ophthalmici (foph; SI Figures S4K,L and S5K). The foramen n. ophthalmici opens into the "lacerate (presphenoid) fossa" *sensu* [6] (Figure 1D), located ventrolaterad from the foramen opticum, between the os laterosphenoidale, os basisphenoidale, os parasphenoidale and septum interorbitale (os laterosphenoidale complex) of the caudomedial wall of the orbit. In dromornithids, the foramen n. ophthalmici is paired with the foramen n. abducentis, which transmits n. abducens (abducent [VI] nerve, see below). The lateral or maxillomandibular (V_2+V_3) branch of the trigeminal ganglion complex, carries n. maxillaris (maxillary [V_2] nerve) and n. mandibularis (mandibular [V_3] nerve), both of which enter the skull rostroventrolaterally at the foramen n. maxillomandibularis (fmx, SI Figures S4K,L and S5K), a single opening between the prootic and laterosphenoid bones of the skull. In dromornithids, the maxillomandibular branch is distinctive in that it is markedly elongate, compared to the extant galloanseres assessed, and transmits the maxillary (V_2) and mandibular (V_3) cranial nerves minimally 20 mm caudoventrolaterally (in *Dromornis*), after entering the skull at the foramen n. maxillomandibularis (see also V_2 + V_3, Figure 3B, SI Figure S5L; and Section 3.2.5 below).

3.1.4. Nervus Abducens

The abducent (VI) nerve inserts on the rostroventral rhombencephalon and is transmitted caudoventrally through the osseus canalis n. abducentis, after entering the skull at the foramen n. abducentis. In dromornithids, the foramen n. abducentis is paired with the foramen n. ophthalmici, forming a single bi-lobal foramen in the rostromedial os laterosphenoidale structures of the orbit (fa, SI Figures S4K,L and S5K; VI, Figure 3B and SI Figure S5L; and above).

3.1.5. Nervus Glossopharyngeus

The glossopharyngeal (IX) nerve inserts caudoventrolaterally on the rhombencephalon (rho; Figure 3A), and forms the rostral component of the combined root ganglion proximale (proximal ganglion; gpr, Figure 3D) with n. vagus (vagus [X] nerve, see below).

The proximal ganglion is enclosed in the fovea ganglii vagoglossopharyngealis in the lamina parasphenoidalis of the fossa cranii caudalis, between the exoccipital and opisthotic bones. The glossopharyngeal (IX) nerve enters the cranium caudoventrolaterad from the vagus (X) nerve at the foramen n. glossopharyngeus (fg; SI Figure S4M,N), situated in the fossa parabasalis. In dromornithids, the glossopharyngeal (IX) and vagus (X) nerves separate caudoventrolaterad of the eminence of the proximal ganglion from the rhombencephalon surface (Figure 3D). The separation of the glossopharyngeal (IX) and vagus (X) nerves in dromornithids is similar to, but occurs to some extent further distally, than the condition seen in *Anhima cornuta* (Figure 4D), *Gallus gallus* (Figure 4H), and *Anseranas semipalmata* (Figure 4P), but distinct to that seen in *Leipoa ocellata* (Figure 4L).

3.1.6. Nervus Hypoglossus

The hypoglossal (XII) nerves typically comprise rostral (XIIr) and caudal (XIIc) rami (e.g., Figure 4D,H,L,P), which in dromornithids are represented by one ramus at either side of the caudoventrolateral medulla oblongata (e.g., XII, Figure 3D,H,L). This condition is distinct to that seen in *A. cornuta* (Figure 4D), *G. gallus* (Figure 4H), *L. ocellata* (Figure 4L), and *A. semipalmata* (Figure 4P), which display both rostral (XIIr) and caudal (XIIc) hypoglossal rami. In dromornithids, the nerves appear to transmit through a single canalis n. hypoglossi and bifurcate in close proximity with the external surface of the os exoccipitale, at the paired foramen n. hypoglossi (fh, SI Figure S4M,N).

3.2. Characteristics of Dromornithid Endocast Morphology

3.2.1. Rostral Telencephalon

The external morphology of the rostral telencephalon as defined here (see SI Figures S10 and S11 and Section S3.2.1.3), evident rostrodorsally of the medial cerebral artery (acm, see Figure 3A,B and Figure 4B,D) in both anseriforms, and somewhat less so in the galliforms, is notably absent in dromornithids. We prefer the explanation that the rostral telencephalon in dromornithids have been masked by hypertrophy of the wulst (see below), and that the external remnants of rostral telencephalon morphology are only visible, in rostral aspect, as twin eminences ventromediolaterad of the olfactory bulb, on either side of the rostromedial surface of the dromornithid endocast (e.g., tel.r; Figure 3B,D).

3.2.2. Wulst

The wulst in dromornithids are greatly hypertrophied and dominate the entire dorsal endocast morphology (see wlst, Figure 3B,D). They extend rostromediolaterally to effectively mask the olfactory bulbs (see Section 3.1.1 above), and extend rostroventrally over the most rostral eminence of the rostral telencephalon, substantially overhanging the rostroventral surface of the brain when viewed from the ventral aspect (Figure 3D,H,L). The wulst extend rostrolaterally and mask the rostrodorsal telencephalon (see above, Figure 3), obscuring the rostrodorsal endocast morphology visible in the extant galloanseres (e.g., Figure 4). The wulst extend mediolaterally across the entire dorsal forebrain, to the lateral vallecula transition zones delimiting the boundaries between the mediolateral wulst, and the dorsolateral caudal telencephalon (see Section 3.2.3 below). The vallecula transition zones are well defined, as the wulst are strongly dorsolaterally expanded in those areas (va, Figure 3B,C). Caudodorsally, the wulst grade into the cerebrum pars occipitalis (coc, Figure 3C) in the region of the medial glandula pinealis (gp, Figure 3A,C), rostrolaterad of the dorsomedial cerebellum (Figure 3C). Notably, dromornithid wulst structures are located somewhat rostrally on the dorsal endocast (e.g., Figure 3C,G,K), such that they do not overlap the rostromedial eminence of the cerebellum when viewed from the lateral aspect (e.g., Figure 3A,E,I); this is similar to the condition in *A. cornuta* (Figure 4A,C), *G. gallus* (Figure 4E,G), *L. ocellata* (Figure 4I,K), and distinct to the condition seen in the anseriform *A. semipalmata* (Figure 4M,O).

3.2.3. Caudal Telencephalon

The caudal telencephalon in dromornithids are well defined and are delimited from the wulst by the vallecula transition zone dorsolaterally (va, Figure 3B,C). The mediolateral hypertrophy of the caudal telencephalon begins approximately where the medial cerebral artery traverses the telencephalic hemisphere dorsoventrolaterally (acm, Figure 3A,B). They extend ventrolaterally, approximately level (dorsoventrally) with the fissura subhemispherica (fs, Figure 3B), and return medially, somewhat acutely, to grade into the ventrolateral optic lobe (see below). Caudally, the cerebrum pars occipitalis (coc, Figure 3C) forming part of the dorsal caudolateral caudal telencephalon, grades into the dorsorostrolateral pons and medulla oblongata structures forming the overall metencephalon complex rostromediad of the cerebellum, in the vicinity of the glandula pinealis dorsolaterally, and medially at the rostromediolateral metencephalon.

3.2.4. Optic Lobe

The optic lobes in dromornithids are somewhat visually inconspicuous structures in comparison to those in the extant galloanseres (opt, Figure 3B vs Figure 4B,F,J,N). They are defined by a slight lateral hypertrophy of the ventromedial endocast ventrolaterad of the fissura subhemispherica, and rostrally by transition into the caudolateral chiasma opticum and tractus opticus structures. Caudally, the optic lobes grade into the ventromediolateral metencephalon complex (see below, Figures 3 and 4).

3.2.5. Trigeminal Ganglia

Trigeminal ganglia receive the three divisions of the trigeminal nerve (V, see Section 3.1.3 above), and insert on the ventral surface of the optic lobe (tri.g, Figures 3D and 4A,D). The trigeminal ganglia form part of the Modular Slm suite, therefore, are described here (see SI Figures S10 and S11, Section 2.6.1 and Section S3.2.1.9). In dromornithids, the medial portion of the trigeminal ganglion carrying the ophthalmic nerve (V_1) separates from the lateral branch carrying the maxillary (V_2) and mandibular (V_3) nerves and exhibits a small ganglionic bridge between the two primary eminences (Figure 3D,H,L). The characteristics of dromornithid trigeminal ganglia are distinctive in that the maxillomandibular branch transmits minimally 20 mm caudoventrolaterally (in *Dromornis*), after entering the skull at the foramen n. maxillomandibularis.

3.2.6. Cerebellum

The cerebellum, as reflected in the endocast in dromornithids, is compressed rostrocaudally and expanded mediolaterally (Figure 3C,G,K), and more so in species of *Dromornis*. From the lateral aspect (see Figure 3A,E,I), the dorsal rostroventral surface forms a shelf somewhat level with the dorsal lateral semicircular duct (dsl, Figure 3B,D) of the vestibular organ (lv, Figure 3A), before turning sharply ventrally in the vicinity of the dorsolateral auricula cerebelli, to grade into the caudodorsal medulla spinalis at the osseous foramen magnum. Overall, the exposed dromornithid cerebellum and the associated ventral rhombencephalon (medulla oblongata + pons; see below), compared with the extant galloanseres, form a comparatively distinctive hind brain in these birds.

3.2.7. Rhombencephalon

Rhombencephalon is the collective term describing the structures of the medulla oblongata and pons, forming the caudoventrolateral areas of the hindbrain. In dromornithids, the ventral rhombencephalon surface is somewhat flat rostrocaudally and mediolaterally (i.e., not as ventrally curved as in other galloansere specimens, e.g., Figure 4), and extends further rostrocaudally than it does mediolaterally.

3.3. Key Morphological Differences between Species of Dromornis and Ilbandornis

In the following, we present a summary of results for Modular Lm data, Measurement data, and Surface Area data forms. Full descriptions of results are given in SI (see SI Sections S4 and S5).

3.3.1. Wulst Modules

The overall size and surface area of the wulst increased between the late Oligocene and the middle Miocene in species of *Dromornis*, particularly rostrodorsally, and in the ventrolateral displacement of the vallecula transition zones between the dorsolateral wulst and the dorsal caudal telencephalon (see SI Section S4.1.1). The wulst in *D. stirtoni* likely had a comparable dorsal profile to other species of *Dromornis*, in that the rostrocaudal and mediolateral profile is distinctively hypertrophied (see SI Section S4.2.1). The late Oligocene *D. murrayi* and middle Miocene *I. woodburnei* dromornithids have similar length ratios, but the mediolateral width ratio is markedly smaller in *D. murrayi*. Similarly, results for Surface Area data show that *D. murrayi* has a smaller wulst surface area ratio than *I. woodburnei* (see SI Section S4.4.1).

With respect to the middle Miocene dromornithids, *D. planei* shows greater rostrodorsal hypertrophy of the wulst, and the dorsolateral margin of the vallecula transition zones are more ventrolaterally located than in *I. woodburnei*. *D. planei* has greater overall rostrocaudal length and caudal mediolateral width ratios than *I. woodburnei*. These results are consistent with those for Surface Area data, which show *D. planei* has a larger surface area ratio than *I. woodburnei* (see SI Section S4.3.1). *Ilbandornis woodburnei* displays a deeper fissura interhemispherica transition zone, placing the medial wulst margins closer together than in both species of *Dromornis* assessed.

3.3.2. Caudal Telencephalon Modules

The overall size and surface area of the caudal telencephalon reduced between the late Oligocene and the middle Miocene in species of *Dromornis* (see SI Section S4.1.2), and between species of *Dromornis* and *Ilbandornis* (see SI Sections S4.3.2 and S4.4.2). However, the characteristic shape of the structures are maintained within the late Oligocene through middle Miocene species of *Dromornis*. The caudal telencephalon of the late Miocene *D. stirtoni* is mediolaterally hypertrophied and is similar to the other species of *Dromornis* (see SI Section S4.2.2). The main differences in the caudal telencephalon between species of *Dromornis* and *I. woodburnei*, are that caudoventral margins project further ventrally in species of *Dromornis*, this is reflected in caudal telencephalon dorsoventral width ratios being greater in species of *Dromornis* than in *Ilbandornis*.

3.3.3. Cerebellum Module

There was limited rostrodorsal hypertrophy in the cerebellum between the late Oligocene and the middle Miocene in species of *Dromornis*. The dorsal surface of the cerebellum in the late Miocene *D. stirtoni* has a similar rostrocaudal shape to the other species of *Dromornis*, but the dorsal cerebellum appears more ventrally orientated in *D. stirtoni* (see SI Section S4.2.3). Species of *Dromornis* and *Ilbandornis* differ notably in the shape of the cerebellum, where species of *Dromornis* have mediolaterally wider and rostrocaudally shorter cerebellum profiles.

The middle Miocene species *D. planei* and *I. woodburnei* have a larger cerebellum than the late-Oligocene *D. murrayi* (see SI Sections S4.1.3, S4.4.3). Additionally, *I. woodburnei* displays a rostrocaudally longer and mediolaterally narrower cerebellum profile than both species of *Dromornis* (see SI Sections S4.3.3 and S4.4.3). It is notable, however, that there exist rostrocaudolateral profile similarities between the cerebellum of the middle Miocene *D. planei* and *I. woodburnei* specimens, that differ from the late Oligocene *D. murrayi*. Where both middle Miocene species display relative hypertrophy of the rostrodorsal through dorsomedial cerebellum, affecting a rostrocaudally steeper caudal transition to the dorsal medulla spinalis, compared to the older *Dromornis murrayi*.

3.3.4. Rhombencephalon Module

There was a dorsal displacement of the rhombencephalon surface between the late Oligocene and the middle Miocene in species of *Dromornis*, and the development of an overall 'flatter' mediolateral and rostrocaudal rhombencephalon profile in *D. planei.* As noted for the cerebellum above, the rhombencephalon structure in *D. stirtoni* appears to be more ventrally situated than that of *D. planei*. These observations suggest that the apparent ventral displacement of the dorsal cerebellum and ventral rhombencephalon surfaces in *D. stirtoni*, may reflect a compensatory ventral rotation of the hindbrain complex, with respect to the rostrodorsal rotation evident in the forebrain (see SI Section S4.2.4). In effect, the brain of *D. stirtoni* appears rotated about the median plane, whilst the position of the dorsomedial surfaces of the brain have been maintained, effectively foreshortening the overall rostrocaudal length of the *D. stirtoni* endocast compared with other species of *Dromornis*.

The overall length of the rhombencephalon between species of *Dromornis* and *Ilbandornis* are remarkably similar. However, in species of *Dromornis*, the rhombencephalon describes a more 'flat' rostrocaudal profile, along with greater mediolateral width ratios compared to *I. woodburnei*. The surface area ratio of the rhombencephalon in *D. planei* is markedly larger than that of *I. woodburnei* (see SI Section S4.3.4), and the late-Oligocene *D. murrayi* has a larger ratio compared with the middle Miocene *I. woodburnei* (see SI Section S4.4.4). These trends are similar to those noted in the comparisons of *D. planei* and *I. woodburnei* (see SI Section S4.3.4, and above), and suggest that the size of the cerebellum may have increased, particularly in the rostromedial zone, across both *Dromornis* and *Ilbandornis* lineages between the late Oligocene and the middle Miocene. However, this observation may only be tested by assessment of yet to be discovered cranial material of the *Ilbandornis* lineage from the late Oligocene.

3.4. Key Morphological Differences between Dromornithids and the Extant Galloanseres

3.4.1. Innervation

Unlike in dromornithids, the olfactory zones of extant galloanseres are wholly external to the rostral telencephalon, as revealed by their slight constriction immediately rostrad of the rostral telencephalon, particularly evident in *A. semipalmata* (Figure 4M,O,P) and *A. cornuta* (Figure 4A,C,D). The hypoglossal (XII) nerves have a single origin at either side of the caudoventral medulla oblongata in dromornithids, this condition is unlike the extant galloanseres, which display rostral (XIIr) and caudal (XIIc) rami (Figure 4D,H,L,P). Results for Measurement data show the trigeminal ganglia of *A. semipalmata* and *A. cornuta* are wider than those of all other galloanseres. Surface Area data show the galliforms *L. ocellata* and *G. gallus* have the smallest surface area ratios for the face of the maxillomandibular ($V_2 + V_3$) branch of the trigeminal (V) nerve, closely followed by the dromornithids. The anseriforms *A. semipalmata* and *A. cornuta*, respectively, have the largest maxillomandibular surface area ratios for all galloanseres assessed (see SI Section S5.1).

3.4.2. Wulst Modules

Wulst modules in extant galloanseres are much hypotrophied in comparison with all dromornithids (e.g., Figure 3 vs Figure 4). Results for Measurement data show *G. gallus* has the shortest and narrowest wulst ratios, followed by *L. ocellata*, and the anseriforms *A. cornuta* and *A. semipalmata*, respectively. Dromornithids have substantially larger wulst surface area ratios than all galloanseres, but when endocast absolute size is accounted for, *G. gallus* and *L. ocellata* have the largest wulst surface area ratios among the extant galloanseres, and the anseriforms *A. cornuta* and *A. semipalmata* the smallest, respectively (see SI Section S5.2).

3.4.3. Rostral Telencephalon Modules

Evidence of the rostral telencephalon is conspicuously absent on the external morphology of dromornithid endocasts, and only present rostrally as twin eminences ventromedi-

olaterad of the olfactory bulb, on either side of the rostromedial surface of the endocast (tel.r, Figure 3B,D). Consequently, detailed comparisons were not possible between the rostral telencephalon of dromornithids and those of the extant galloanseres, and we present results for the extant galloanseres only. Measurement data show *G. gallus* has the shortest and narrowest rostral telencephalon ratios, followed by *L. ocellata*, and the anseriforms *A. cornuta* and *A. semipalmata*, respectively. Similarly, results for Surface Area data show that *G. gallus* has the smallest surface area ratio, and *A. semipalmata* the largest surface area ratio of all extant galloanseres (see SI Section S5.3).

3.4.4. Caudal Telencephalon Modules

Results for Measurement data show that all dromornithids have relatively greater rostrocaudal length ratios compared with the extant galloanseres. However, all extant galloanseres overlap in dorsoventral width ratios. Dromornithids have the greater mediolateral endocast total width ratios of all galloanseres, and the galliforms have somewhat similar endocast total width ratios as the anseriform *A. semipalmata*.

Results for Surface Area data show that the dromornithids have the largest surface area ratios of all specimens, *L. ocellata* has the smallest surface area ratio of all specimens, and the phasianid *G. gallus* has the largest surface area ratio of the extant galloanseres (see SI Section S5.4).

3.4.5. Optic Lobe Modules

Results for Measurement data show the extant galliforms have the largest optic lobe length and width ratios, followed by the anseriforms and dromornithids. Results for Surface Area data (see SI Section S5.5) show that the largest taxa have the smallest overall optic lobe ratios, and reveal the optic lobe in *I. woodburnei* is larger than those of both species of *Dromornis*. Surface Area ratios for the anseriforms *A. cornuta* and *A. semipalmata* are somewhat similar to those of the dromornithids, and the galliforms *G. gallus* and *L. ocellata* have the largest surface area ratios of all specimens assessed.

3.4.6. Cerebellum Module

Results for Measurement data show the cerebellum, as exposed in the endocast in dromornithids, are notably rostrocaudally shorter and mediolaterally wider than those of all extant galloanseres, with the width ratio for *A. semipalmata* most approaching those of the dromornithids. Rostrad of the foramen magnum, all extant galloanseres display a gradual rostrolateral divergence of cerebellum mediolateral margins, prior to grading into the cerebrum pars occipitalis regions of the caudal telencephalon. This condition is not evident in dromornithids, which display a more abrupt mediolateral divergence of caudodorsal cerebellum margins, which are more pronounced in species of *Dromornis* than in *I. woodburnei*. Results for Surface Area data show that the dromornithids have the largest ratios of all galloanseres. Among the extant galloanseres, *A. semipalmata* has the smallest surface area ratio for all specimens. *Leipoa ocellata* overlaps with those of the dromornithids, and is most similar to that of *I. woodburnei*. *Anhima cornuta* has a larger surface area ratio than all dromornithids, and the *G. gallus* has the largest surface area ratio of all galloanseres (see SI Section S5.6).

3.4.7. Rhombencephalon Module

Results for Measurement data show that all galloanseres have somewhat similar rhombencephalon length ratios, with the exception of *A. cornuta*, which has the largest rostrocaudal length ratio of all galloanseres. Rhombencephalon width ratios for extant galloanseres are all larger than in dromornithids, and likely reflect the greater ventral projection, or eminence, of the rhombencephalon in the extant specimens. The overall mediolateral width ratio of the hindbrain in species of *Dromornis* are greater than in all galloanseres assessed, and that of *I. woodburnei* overlaps with those of the extant galloanseres. Results for Surface Area data show that the dromornithids *I. woodburnei* and *D. murrayi*

have the smallest rhombencephalon surface area ratios, followed by *A. semipalmata* and *G. gallus*. The dromornithid *D. planei* has a somewhat similar surface area ratio as *G. gallus*, and *A. cornuta* and *L. ocellata* have the largest surface area ratios among all galloanseres (see SI Section S5.7).

4. Discussion

Dromornithid endocranial anatomy is described here in detail for the first time, using specimens from fossil sites in Australia spanning ~20–8 Ma. In the following, (1) we summarise the morphological characteristics of the dromornithid brain, and discuss these features with respect to those of exemplars of other major galloansere clades; (2) we review potential lineage-specific morphological characteristics identified in dromornithid endocranial anatomy; (3) we comment on morphological changes observed to have occurred in the endocranial anatomy of the *Dromornis* lineage over time; (4) we assess potential functional implications of the dromornithid endocranial condition.

4.1. Comparisons of Endocranial Characteristics of Dromornithids and Extant Galloanseres

4.1.1. Olfactory Bulb

The olfactory bulb in dromornithids is pronounced both dorsally and ventrally in the oldest (*Dromornis murrayi*) species. However, in middle Miocene specimens (*D. planei* and *Ilbandornis woodburnei*), its dorsal morphology is masked by the rostral eminence of the wulst (see Section 4.1.3 below). There appears no reduction in the size of the olfactory bulb in the younger dromornithids, as from the ventral aspect, lateral margins of the organ transition into the rostroventral endocast without reduction in mediolateral width. In extant galloanseres, the olfactory bulb of *Anseranas semipalmata* displays hypertrophy in excess of that seen in *Anhima cornuta*, which is somewhat more than those of *Leipoa ocellata* and *Gallus gallus*. The olfactory zones of these galloanseres appear wholly external rostrad of the rostral telencephalon, as the olfactory bulb margins constrict somewhat prior to grading caudally into the rostral telencephalon, a condition distinct from those of dromornithids.

Taken together, the evidence shows that the wulst extends rostromediolaterally to effectively mask the olfactory bulbs in dromornithids, and so contrary to a first assessment that might consider that dromornithids had hypotrophied olfactory bulbs, we consider them to be relatively no smaller than in the other galloanseres.

4.1.2. Trigeminal Ganglia

Trigeminal ganglia transmit the three divisions of the trigeminal (V) nerve complex and insert on the ventral surface of the optic lobe. They are distinctive in dromornithids, in that the maxillomandibular (V_2 + V_3) branch passes minimally 20 mm caudoventrolaterally through the unusually thick cranium (in *Dromornis*), after entering it at the foramen n. maxillomandibularis. The extended transmission of the maxillomandibular branch through the cranium in dromornithids accommodates for the unusually thick honeycomb-like trabecular bone separating the cortical bone defining the endocranial capsule, from the outer cortical cranial surface (e.g., SI Figure S8I). In the extant galloanseres, the transmission of these nerves from the foramen n. maxillomandibularis is markedly shorter. Notably, however, in the phasianid galliform *G. gallus* (see Figure 4E,F,H), the transmission of the maxillomandibular (V_2 + V_3) branch through the cranium, although somewhat shorter than that observed in dromornithids, is longer than observed in the other extant galloanseres. Moreover, CT data for *G. gallus* reveals that this is also accompanied by trabecular matrix surrounding the endocranial capsule through which the nerves transmit [Pers. Obs. Authors].

In general, the shape of the avian cranium, particularly dorsally, exhibits a close relationship to the shape of the brain within [68–74]. However, patterns of the brain size 'lagging behind' the body, accompanying an increase in the relative thickness of trabecular bone surrounding the endocranial capsule have been recognised in Haast's eagle *Hieraaetus moorei* (Haast, 1872) by Scofield and Ashwell [75], who showed that the eagle's "ten-fold"

increase in body size was only accompanied by a "doubling or tripling" of endocast volume. This demonstrated lag of neuroanatomy behind rapid hypertrophic skeletal changes in a taxon, may relate to strong selection for body size, i.e., adaptation to a novel trophic niche, or artificial selection in the form of "stringent" human mediated selection for desirable phenotypes (e.g., as in the case of *G. gallus* see [76], and references therein). Consequently, as dromornithids became larger through the course of their evolution (e.g., [6,31]), it is likely the increase in physical size of the cranium, was accommodated for by an increase in trabecular bone enclosing the 'lagging' endocranial capsule [75] (Figure 5a).

Similarly, the *G. gallus* skull used for CT scanning for this project was almost certainly from a domestic chicken, and may demonstrate increasing trabecular thickness in the cranium, mediated by human selection for body size. To assess these observations more comprehensively, additional data in the form of wider sampling across galloanseres in particular, but across Neornithes in general is required, targeting taxa with demonstrated temporal increases in body size.

Results for Measurement data show the trigeminal ganglia of *A. semipalmata* and *A. cornuta* are relatively wider than those of all other galloanseres, and Surface Area data show the galliforms *L. ocellata* and *G. gallus* have the smallest surface area ratios for the face of the maxillomandibular (V_2 + V_3) branch of the trigeminal (V) nerve, closely followed by the dromornithids. The anseriforms *A. semipalmata* and *A. cornuta*, respectively, have the largest maxillomandibular surface area ratios for all galloanseres assessed (see Section 3.4.1). The eminence of the hypoglossal (XII) nerves which typically comprise a rostral (XIIr) and caudal (XIIc) branch in extant galloanseres, is represented by one nerve root at either side of the caudoventrolateral medulla oblongata in dromornithids, with bifurcation into rostral and caudal branches occurring within the os exoccipitale, close to the caudomediolateral surface of the cranium.

4.1.3. Wulst

The morphology of the wulst is the most distinguishing feature uniting dromornithids, forming massively hypertrophied structures. The wulst extends rostromediolaterally to effectively cover the olfactory bulbs and extends rostroventrally over the most rostral eminence of the rostral telencephalon, substantially overhanging the rostroventral surfaces of the brain. The dromornithid wulst extend strongly rostrolaterally, masking the rostrodorsal telencephalon (see Section 4.1.4 below), and extends mediolaterally across the entire dorsal forebrain. The structure of the wulst in dromornithids is unlike any seen in the extant galloanseres. Results show the dromornithids all display much larger width and length, and surface area ratios, than all the extant galloanseres. When endocast absolute size is accounted for, *G. gallus* and *L. ocellata* have the largest wulst surface area ratios among the extant galloanseres, and the anseriforms *A. cornuta* and *A. semipalmata* the smallest (see Section 3.4.2).

Among taxa that were not included in these analyses, some palaeognaths display hypertrophy of the wulst. For example, Corfield et al. [49] (Figure 1B–E) figured endocasts of the extinct NZ moa *Dinornis novaezealandiae* Owen, 1843 and *Anomalopteryx didiformis* (Owen, 1843), and those of extant ratites like emu (*Dromaius novaehollandiae*) and ostrich (*Struthio camelus*). Additionally, Ashwell and Scofield [77] (Figure 6G–I) figured the dorsal endocasts of several NZ moa: *D. robustus* (Owen, 1846), *A. didiformis*, *Euryapteryx curtus gravis* (Owen, 1870), and *Emeus crassus* (Owen, 1846) as well, all of which show wulst characteristics similar to those seen in dromornithids, wherein the vallecula, especially in the larger moa taxa, visibly extend rostrocaudally across the entire dorsolateral telencephalic hemispheres. These characteristics suggest that such characteristic hypertrophy of the wulst in large flightless birds (see also [78] (Figures 1 and 2), [79] (Figure 2a), [80] (Figures 1 and 3), [81] (Figure 1), [74] (Figures 5.3 1–6), may represent a parallel convergent modification towards enhanced visual proficiency and stereoscopic capability (see also Section 4.4.2.1 below). However, ratite taxa clearly display a lesser degree of wulst hypertrophy than that evident in dromornithids. Even the oldest dromornithid cranial fossils

(e.g., *D. murrayi* from the ~20 Ma sites of Riversleigh), display greater hypertrophy of the wulst than seen in any ratite, indicating a long dromornithid "ghost lineage" must have existed prior to any substantive fossil evidence of dromornithids in Australia (see also [6] (p. 19)). Evidence for such, comprise trackways reported from the late Oligocene of Tasmania [1], postcranial remains from the late Oligocene Pwerte Marnte Marnte LF in the Northern Territory [4], and a mould of fossil footprints from the Eocene Redbank Plains Formation of Queensland [7].

4.1.4. Rostral Telencephalon

Evidence of the rostral telencephalon in dromornithids is only present rostroventrally as twin eminences ventromediolaterad of the olfactory bulb, on either side of the rostromedial endocast (tel.r; Figure 3B,D). It is possible that these eminences are expanded cerebrum tuber ventrolaterale structures, as evident in *A. cornuta* (Figure 4A,B,D). However, their interpretation as remnant rostral telencephalon eminences is favoured, as in all dromornithid endocasts modelled, there exist pronounced paired eminences in this rostromedial zone that are not present to the same degree in any avian endocast modelled or observed in the literature [Pers. Obs. Authors]. Further support for this, is that the positioning of these rostral eminences in dromornithids, agrees with the angle and position of rostral telencephalon eminences in specimens, when endocasts are aligned to putative "alert posture" [82–85], with reference to the horizontal positioning of the lateral semicircular canal of the vestibular organ. Additionally, the rostrocaudal transition angle of the vallecula, describing the dorsal margins of the caudal telencephalon, agree with the extension of the visible rostral eminences of the dromornithid rostral telencephalon, should the dorsolateral curve of the rostral telencephalon not be masked by hypertrophy of the rostromediolateral wulst. In support of this interpretation, the apparent rostral extension of the vallecula across the dorsolateral surface of moa endocasts figured by Ashwell and Scofield ([77] Figures 5E−5I and 6G–6I) and Corfield et al. ([49] Figure 1b D–E), and similarly in the brains of extant flightless ratites (see [78] (Figures 1 and 2), [79] (Figure 2a), [77] (Figure 6), [49] (Figure 1B,C), [80] (Figures 1 and 3), [81] (Figure 1), [74] (Figures 5.3 1–6)), suggest that the evolution of a rostromediolaterally hypertrophied wulst in large flightless birds may effectively mask rostral telencephalon morphology. The accommodation of this apparently major change in rostrodorsal endocranial morphology in dromornithids, would have necessitated a dorsomedial displacement of the olfactory bulb, which we think is a possibility, as this condition is somewhat similar to that seen in moa (e.g., [77] (Figures 5e–l and 6g–l), [49] (Figure 1b D–E)).

Detailed comparisons of the dromornithid rostral telencephalon were not possible. However, results of comparisons among extant galloanseres show the phasianid *G. gallus* has the smallest rostral telencephalon, followed by the megapodiid *L. ocellata*, and the basal anseriform *A. cornuta*. The anseriform *A. semipalmata* has the most hypertrophied rostral telencephalon of the extant galloanseres (see Section 3.4.3).

4.1.5. Caudal Telencephalon

The caudal telencephalon is strongly defined in all galloanseres assessed. Results show dromornithids have relatively greater rostrocaudal length and mediolateral endocast total width ratios than the extant galloanseres. Similarly, the dromornithids have the largest caudal telencephalon surface area ratios, and the megapodiid *L. ocellata* has the smallest surface area ratio of all specimens. The phasianid *G. gallus* has the largest surface area ratio for the extant galloanseres (see Section 3.4.4).

4.1.6. Optic Lobe

The optic lobe in dromornithids appear somewhat indistinct, and not as well delimited as in the extant galloanseres. This is confirmed by results revealing the extant galliforms have the largest optic lobe length and width ratios, followed by the anseriforms and dromornithids. These patterns are also reflected by results for Surface Area data which

show the dromornithids have the smallest optic lobe surface area ratios, followed by those of the anseriforms. The largest surface area ratios for all galloanseres assessed are shown by the galliforms *G. gallus* and *L. ocellata*. Overall, results show that when endocast size is accounted for, the largest overall taxa display the smallest overall optic lobe ratios, and reveal relatively greater hypertrophy of the optic lobe in the *Ilbandornis* lineage compared with species of *Dromornis* (see Section 3.4.5).

Additionally, during the process of segmenting the endocast models used for this project, we retained trigeminal ganglion structures (see Figure 3D,H,L) inserting on the ventral surfaces of the optic lobe, primarily to gain insight of dromornithid somatosensory capabilities (e.g., Section 4.4.1 below). This, however, resulted in the ventromedial surfaces of optic lobe Slm modules being constrained by the morphology of the trigeminal ganglia. Retrospectively, it may have been more useful to segment the trigeminal (V) complex out of the final endocast models, enabling access to the full extent of the ventral optic lobes and allowing consideration of optic lobe morphology with respect to those of the wulst and optic foramen (*sensu* [50]; see also [86], and (Section 4.4.2.3 below). This aspect of dromornithid cranial morphology forms part of continuing work on the brains of these giant birds.

4.1.7. Cerebellum

Dorsal cerebellum margins in dromornithids are characteristically rostrocaudally compressed and mediolaterally expanded. Results show that the exposed cerebellum in dromornithid endocasts are rostrocaudally shorter and mediolaterally wider than those of all extant galloanseres. Results for Surface Area data show that the galliform *G. gallus* has the largest cerebellum ratio, and the anseriform *A. semipalmata* the smallest ratio of all galloanseres assessed. *Dromornis planei* has the largest cerebellum surface area ratio of the dromornithids, and the ratios for *A. cornuta* and *L. ocellata* overlap with those of dromornithids. Rostrad of the foramen magnum, all extant galloanseres display a gradual rostrolateral divergence of cerebellum mediolateral margins, prior to grading into the cerebrum pars occipitalis regions of the caudal telencephalon. This condition is not evident in dromornithids, which display a much more abrupt mediolateral divergence of the caudodorsal cerebellum margins, and this is more pronounced in species of *Dromornis* than in *Ilbandornis*. Progressing rostrally, dromornithid cerebellum margins describe a somewhat parallel rostrocaudal transition (see Section 3.4.6).

4.1.8. Rhombencephalon

Dromornithids display relatively flat ventral rhombencephalon surfaces rostrocaudally and mediolaterally, whereas, in comparison, all extant galloanseres show much ventrally hypertrophied rhombencephalon surfaces (rho; Figure 4A,B,D). These trends are reflected by results for Measurement data showing all galloansere species, with the exception of *A. cornuta*, have similar rhombencephalon length ratios. Width ratios for the extant galloanseres are all larger than those of the dromornithids, and likely reflect the greater ventral projection, or eminence, of the rhombencephalon in the extant taxa. The overall width ratio of the hindbrain in species of *Dromornis*, are greater than in all other species, and that of *I. woodburnei* overlaps with those of the extant galloanseres. Results for Surface Area data show that the dromornithids *I. woodburnei* and *D. murrayi* have the smallest surface area ratios, followed by the anseranatid *A. semipalmata* and phasianid *G. gallus*. *Dromornis planei* has a somewhat similar surface area ratio as *G. gallus*, and *A. cornuta* and *L. ocellata* have the largest surface area ratios among all galloanseres assessed (see Section 3.4.7).

4.2. Endocranial Morphology Distinguishing Lineages within Dromornithids

The examination of dromornithid endocasts has revealed morphological features of the dromornithid brain that may provide support for the two-lineage hypothesis (*sensu* [6]). We define these distinctive endocranial attributes below, with a focus on the morphological differences between *Ilbandornis woodburnei* and the two species of *Dromornis* with adequate

preservation for comparison (i.e., *D. planei* and *D. murrayi*): (1) the medial boundaries of the wulst in the rostrocaudal fissura interhemispherica zone of the dorsal endocast in *I. woodburnei*, are notably closer together than in species of *Dromornis*; (2) the most ventral eminence of the *I. woodburnei* caudal telencephalon, in the zone of the fissura subhemispherica, are conspicuously less ventrally pronounced than in species of *Dromornis*; (3) the rostrodorsal cerebellum in *I. woodburnei* defines a more rostrally projecting mediolateral curve than in species of *Dromornis*, which display a flatter rostral dorsomediolateral margin; (4) the caudodorsal part of the cerebellum in *I. woodburnei* projects further caudally in the region of the dorsal medulla spinalis, whereas this region is caudally shorter but mediolaterally flatter in species of *Dromornis*; (5) the entire hindbrain (rhombencephalon, medulla oblongata and metencephalon complex [cerebellum + pons]) in *I. woodburnei*, is rostrocaudally longer and mediolaterally narrower than in species of *Dromornis*.

These morphological traits are potential lineage-specific endocranial attributes, but require confirmation through a shared presence in yet to be discovered crania of *Ilbandornis lawsoni* and *Barawertornis tedfordi*, or in presently undescribed material of *Genyornis newtoni*.

4.3. Temporal Changes in the Endocranial Morphology of the Dromornis Lineage

Across the ~10 Ma period represented by specimens of Oligo–Miocene *D. murrayi*, and the middle Miocene *D. planei*, the orientation of the brain within the skull appears to have remained much the same, despite foreshortening of the cranium. Other than regional changes in endocast shape, for example, the rostrodorsal hypertrophy of the wulst, accompanying other trends described above, the brains of these species are generally similar, and distinctively dromornithid. The relatively major increase in the overall size of species of *Dromornis*, reflected by crania of *D. murrayi* and *D. planei* figured here (e.g., Figure 1A–D; SI Figures S1A–P and S4A–H), and postcranial fossils described elsewhere [1,6], appear to have not been substantial enough to affect changes in the position and orientation of the brain in *D. planei* relative to that of *D. murrayi*. However, by the late Miocene, some ~6 Ma after the occurrence of *D. planei*, the cranium of the *Dromornis* lineage had evolved to become even more foreshortened and dorsoventrally deeper, as manifested in *Dromornis stirtoni* (Figure 1E; SI Figures S6 and S7; see also [6]). These morphological changes appear to have affected the orientation of the brain.

With regard to *D. stirtoni*, it is unfortunate that the state of preservation of specimens prevented the level of endocast shape assessment achieved for the other dromornithids. This was primarily due to the taphonomic characteristics of the only site preserving these giant birds (see Section 2.2 above). In turn, this limited the biological and functional inferences derived from their exceptional cranial architecture. However, we have shown from the similarity of preserved features of the *D. stirtoni* endocast models with those of *D. planei* (see SI Sections S2.1 and S4.2), that the brain of *D. stirtoni* does not depart greatly from the only other known dromornithid endocast morphology. However, the altered endocranial alignment to 'fit' the brain in the foreshortened cranium, resulted in rostroventral endocast surfaces in *D. stirtoni* being rotated rostrodorsally around the medial caudal telencephalon into a more dorsally orientated position. Additionally, it appears the brain of *D. stirtoni* has experienced a measure of dorsoventral compression and mediolateral expansion. These changes in the forebrain are accompanied by a more ventrally orientated hindbrain, which may reflect a compensatory ventral rotation of the hindbrain complex in the species, although the 'life position' of the midbrain in the skull of *D. stirtoni* has not changed appreciably from that of *D. planei*.

The reasons for this unusual rotation and apparent subtle compression of the *D. stirtoni* endocast may lie in the highly derived state of cranial morphology attained by this, the largest of the dromornithids, by the late Miocene. The cranium of *D. stirtoni* is unique in that the rostrocaudal cranial length is effectively about half the cranial depth, and represents the terminal state of a concerted trend in cranial foreshortening, along with an increase in bill size, of the most extreme avian cranial specialisation known [3,6]. This trend extends

from the oldest known species of *Dromornis*, the Oligo–Miocene *D. murrayi*, through the middle Miocene *D. planei*, to the most derived late Miocene taxon *D. stirtoni*.

4.4. Functional Implications of Dromornithid Endocranial Morphology

Jerison [87] (p. 8) proposed the "Principle of Proper Mass" which specifies particular sensory specialisations in the vertebrate brain are correlated with concomitant hypertrophy of the neural tissue processing related information, and that the relative mass of functional neural tissue implies the relative importance of those functions in the species. Subsequent studies showed that overall brain size was in fact increased by independent hypertrophy of particular brain regions (see [88–91], and references therein), supporting Jerison's [87] observations, which became to be known as the "mosaic" model of brain evolution (*sensu* [90]).

That mosaic evolution characterises some, but not all, of avian brain composition has been demonstrated by several works (see [49,92], and references therein). It is acknowledged that the brain is not strictly compartmentalised into regions that process exclusive neuronal input, but rather includes levels of interconnectivity across the whole structure [92]. It is clear that particular brain nuclei share greater levels of neuronal connectivity associated with specific functions; that a hypertrophied brain region reflects a greater level of "information-processing power", and that these patterns are somewhat indicative of functional specialisation ([49,90,93–95] and references therein). Most recently, Early et al. [50] showed there exists statistically significant correlations between the external surface area of the wulst and optic lobe, and the volume of underlying brain regions.

4.4.1. Innervation

Characteristic mosaic correlations in the trigeminal system have previously been shown in several vertebrate taxa (see [96], and references therein). In birds, the trigeminal (V) nerve system comprises the medial portion carrying the ophthalmic (V_1) nerve which innervates the orbit and nasal cavity, the rostral palate and the tip of the upper bill, and forms a major sensory pathway for the skin of the head and maxillary rostrum. The maxillary (V_2) branch innervates the maxillary rostrum and infraorbital regions, and the mandibular (V_3) division innervates the entire lower bill and several mandibular and interramal regions [97–100]. The trigeminal nucleus receives exclusively proprioceptive information from the descending tract, and the principal sensory nucleus of the trigeminal system [96]. This includes not only projections from ophthalmic (V_1) and maxillomandibular (V_2 + V_3) nerves, but taste information from the tongue is conveyed, within the lingual branch of the maxillomandibular (V_2 + V_3) ramus, by the facial (VII) nerve to the trigeminal principal sensory nucleus, which also receives input from glossopharyngeal (IX) and hypoglossal (XII) nerves [93,98,101–105]. In short, the trigeminal (V) nerve comprises the largest somatosensory cranial innervation complex, and transmits epicritic sensation from the entire facial region and mastication musculature [98,105,106]. Dubbeldam [107] proposed that differences in the trigeminal principal sensory nucleus were indicative of the functional demands of specific feeding behaviours. Gutiérrez-Ibáñez et al. [96] reported hypertrophy of the trigeminal principal sensory nucleus in species dependent on tactile input for feeding, and that bill morphology and the concentration of mechanoreceptors in the bill and tongue, strongly correlate with feeding behaviour.

The glossopharyngeal (IX) and vagus (X) nerves share the large proximal ganglion. The glossopharyngeal (IX) components of this complex comprise somatic, "special" and visceral afferent fibres. The special fibres connect with the palatine branch of the facial (VII) nerve at the cranial cervical ganglion, and are associated with sensory taste and tactile information [98,101,108,109]. The general visceral efferent fibres of the glossopharyngeal (IX) nerve supply the oesophagus and crop, exhibit size variability across taxa that show greater "distensibility" of the oesophagus [98], and are notably hypotrophied in taxa that have no crop (i.e., owls and hawks). The glossopharyngeal (IX) nerve complex bifurcates, after separation from the vagus (X) nerve at the proximal ganglion, and transmits, in two

main afferent branches of the lingual and the laryngopharyngeal nerves, as the descending oesophageal nerves, innervating the tongue and the laryngeal muscles, respectively.

The vagus (X) nerve complex is the most extensive of the sensory and motor cranial nerves, wherein there are two groups of motor fibres. The first consists of "general" visceral efferent fibres which innervate the muscles and glands of the thoracoabdominal viscera, including the heart and lungs, etc., and is associated with circulation, respiration and digestion control [98]. The second consists of "special" visceral efferent fibres innervating the muscles of the pharynx and the larynx, reached via branches of the glossopharyngeal (IX) nerve ([98]; for a contrary opinion, see Wild [103] who argued vagus (X) projections are exclusively cardiovascular and pulmonary in function).

The morphology of dromornithid ventral cranial innervation, in the form of the maxillomandibular (V_2 + V_3), glossopharyngeal (IX) and vagus (X) nerves, and results presented here for trigeminal ganglia, are more similar to the species of galliforms. Dromornithid trigeminal ganglia appear less hypertrophied than those of the more derived, and trophic specialist anseriforms too, this is supported by results for Measurement data. Additionally, Surface Area data describing the truncated face of the maxillomandibular (V_2 + V_3) branch of the trigeminal (V) nerve complex, show that the dromornithids have somewhat similar surface area ratios as the galliforms, and which collectively, are much smaller than those of the anseriforms (see Sections 3.4.1 and 4.1.2). The morphology of dromornithid ventral innervation, better represented by the endocast of *Dromornis planei* (see Figure 3A–D), suggests that dromornithids were likely possessed of somewhat better tactile capability than the extant galliforms (e.g., Figure 4H–L), and were likely employing greater levels of sensory input from the bill, palate, and tongue in their trophic behaviour, than the extant galliforms do.

Dromornithids, especially species of *Dromornis*, have extremely large, deep bills, with dorsally prominent, mediolaterally compressed culmens [1,3,6]. The herbivorous diet of dromornithids is well established ([1], and references therein), but musculature for operation of the bill is "surprisingly limited" [6] (p. 19), and suggests that these birds were not capable of a particularly forceful bite [6], *contra* [3] (p. 88). For example, there is no temporal fossa on the side of the cranium for insertion of mandibular musculature, which is thus limited to the fused postorbital-zygomatic processes, and hyper-developed insertions on the orbital wall of the cranium (i.e., ma, SI Figure S4K,L). Moreover, the culmen, while large, has a lightly constructed osseous core that was only partially covered in rhamphotheca (at least it was in species of *Dromornis*), was highly vascularised and likely highly innervated, a combination of features conferring relatively weak biting ability [6]. The large size of the dromornithid culmen, combined with indications that they are not strengthened for food manipulation, suggest that they were primarily utilised for display, and that the distinctive morphology was likely driven by sexual selection, or by thermoregulatory requisites.

Bill architecture suggests that dromornithids were likely not consuming coarse browse requiring strong bite forces, as were some species of moa (see [19], and references therein). This contention can be tested by observations of the collections of gastroliths used to process such food. We were able to analyse total volume of gastroliths and size of stones in complete or partial gizzard stone sets from specimens of *Genyornis newtoni* to infer characteristics of diet [110–113], and showed (see SI Figure S15 and Table S1) that dromornithids selected gastroliths of much smaller diameter, and accumulated them in surprisingly small overall volumes compared with *Dinornis* moa, although the dromornithids were somewhat larger birds. Moreover, the data reveal that *G. newtoni* selected smaller stones than did the smaller extant emu (*Dromaius novaehollandiae*) which occasionally selected remarkably large gastroliths (see also [110] (Table 2), [111] (p. 26)). In fact, when overall body size was accounted for, gastrolith size ratios for the emu were larger than those of *Dinornis robustus*, although accumulated in smaller quantities. Notably, the stout-legged moa (*Euryapteryx curtus gravis*) has very similar gastrolith size and gizzard mass ratios to those of *G. newtoni*. Stout-legged moa are hypothesised to have exploited a diet of soft leaves and fruit, in dry

scrubland and mosaic environments, in contrast to the generalist tree and shrub browsing *D. robustus* moa, the gizzard contents of which have been shown to comprise much coarser, low-quality fibrous leaf and twig material (e.g., [15,114–116] and references therein). Complete dromornithid gizzard stone sets are rarely preserved, but a complete gizzard set is known for the Oligo–Miocene *Dromornis murrayi*, preserved in situ in limestone (see [28] (p. 79)), and which shows only small stones. The gizzard sets measured for the Pleistocene species *Genyornis newtoni*, show they selected similarly small stones. Thus, if gizzard mass and gastrolith size preferences for *G. newtoni* are representative of dromornithids in general, these results suggest that the fibrosity of browse the dromornithids were targeting was likely similar to that of stout-legged moa (i.e., new growth, soft leaves, and fruit), requiring less vigorous mechanical processing in the gizzard [112]. Such a diet would require specialised visual pathways for the identification and selection of specific food resources. We have shown that dromornithids may have had well-developed somatosensory and sensorimotor capabilities, and so were likely adapted for precise and selective visual browsing.

4.4.2. Visual Pathways

There are three principal visual pathways in birds: (1) the thalamofugal pathway transmits visual signals from the retina via the optic lobe, to the principal optic nucleus of the dorsal thalmus, and thence to the wulst; (2) the tectofugal pathway transmits via the optic lobe to the nucleus rotundas of the thalmus, and proceeds to the entopallium of the caudal telencephalon; and (3) the third visual pathway transmits via the optic lobe through retinal recipient nuclei in the accessory optic system and pretectum, and projects to several regions of the brain, including the cerebellum (see [49,117–120], and references therein).

4.4.2.1. Wulst

The wulst are composed of two main regions, the larger "visual" region, located dorsally and extending caudodorsally, which receives retinal projections, and a smaller rostral somatosensory region, receiving "substantial" somatosensory and kinesthetic input [94,106,121–123]. The thalamofugal pathway, incorporating the wulst, has been shown to be primarily involved in binocular vision capability, and global stereopsis ([94,120,124–126] and references therein). Iwaniuk et al. [94] showed that the size of the wulst was significantly correlated with more frontally orientated orbits and broader binocular fields [120,127], and argued changes in the relative size of the wulst were indicative of increases in somatosensory and motor processing capabilities [48,124,128,129]. Additionally, wulst structures are hypertrophied in species that forage using tactile information from the bill [120,124,130,131].

Dromornithids may have had a well-developed thalamofugal pathway as they display particularly hypertrophied wulst structures. Potential indications of the kinds of adaptive selection driving dromornithid wulst morphology, may lie in the extraordinarily similar morphology of avian predators such as Barn owls (*Tyto alba*), and the Australian Tawny frogmouth (*Podargus strigoides*), which have a similarly hypertrophied wulst structures too (e.g., [124] (Plate 26), [120] (Figure 2), [79] (Figure 2c), [49] (Figure 1bK), [132] (Figure 3A,B), [74] (Figures 5.3 34 and 35)). Barn owls are nocturnal, and possess exceptional low-light visual proficiency and binocularity, or stereopsis [133–137]. Similar specialisations typical of low-light and stereoptic visual proficiency have been recognised in the Tawny frogmouth, which have highly developed visual systems [120,124], and are thought to possess stereoscopic vision [125]. Stereoptic proficiency has been shown to facilitate accuracy in nocturnal prey capture in caprimulgid taxa [125], and spatial, or "topographical cues" associated with feeding activities in *Columba* and *Gallus* [126], and corvids [131,138]. Furthermore, it has been advanced that taxa which use tactile information for foraging (see also Section 4.4.2.2 below) show somewhat hypertrophied rostral wulst structures [120,124], likely as the mandibular (V_3) division of the trigeminal (V) cranial nerve, innervating the lower bill (see Section 4.4.1 above), terminates in the rostrodorsal

mesopallial regions of the brain [99,130,139,140]. As such, the development of stereopsis in birds has been linked with the presence of a well-developed wulst, evidence of which is proposed as compelling indications for the presence of stereoscopic vision specialties in fossil material [125] (p. 220).

Therefore, future analyses of dromornithid orbit size, optic foramen and skull orientation may provide additional insights into the hypertrophy noted in wulst structures for these birds. Cranial anatomy unambiguously shows that dromornithids had large, forward facing eyes (see Figure 1; SI Figures S1, S4 and S6; see also [6] (Table 1)). However, inference as to whether dromornithid retinal topography was structurally adapted (i.e., corneal diameter, retinal cell density/type, etc.), for sensitivity to low light conditions, may only be made by interpretation of orbit shape and size from skeletal remains.

In a large study assessing the relationship between corneal diameter and axial length of the avian eye, Hall and Ross [141] showed that species adapted to light-limited (scotopic or crepuscular) habitats, have larger corneal diameters and axial lengths, relative to those active during well-lit (photopic or diurnal) conditions. Hall [142] showed that there exists a close relationship between corneal diameter and axial length of the eye, and that metrics describing the osseous structures of the orbit were "well associated" with photic activity in birds. In support of these observations, several additional studies have shown that in nocturnal birds, eye shape increases relative to skull length, they display larger orbit diameters relative to depth, and orbits are more frontally orientated (e.g., [94,143,144] and references therein, but see also [131]). Animals that exploit low-light environments have evolved in one of two ways: (1) by enlargement and orientation of the visual system (i.e., increasing orbit size and binocular overlap); or (2) they develop enhanced sensitivity of somatosensory and tactile systems (e.g., [144], and references therein). Among ratites, kiwi are the only confirmed nocturnal taxon, and have evolved reduced eye size and distinct endocranial morphology associated with the somatosensory and tactile systems strategy (i.e., (2) see [79,145]). All other ratites are diurnal, as were the extinct NZ moa [77], and inspection of the shape of their brains (e.g., [75] (Figure 2), [79] (Figure 2a,b), [77] (Figure 6g–l), [145] (Figure 1b A–E), [80] (Figures 1 and 3), [81] (Figure 1), [74] (Figures 5.3 1–6)), show rostromediolaterally hypertrophied wulst structures in these large flightless birds, which may represent evolution for enhanced visual proficiency (i.e., strategy (1) above). However, no ratites display the massively hypertrophied state of the wulst seen in dromornithid dorsal endocasts.

Martin [131] advanced that binocular vision in birds may be used for the inspection of food items held in the bill, for bill control during the process of foraging and food provision to chicks, and not primarily for stereopsis. He also argued that binocular vision in the control of locomotion is a secondary function, as spatial information may be provided by each eye independently. Considering dromornithid cranial morphology displays large, forward facing orbits, and their dorsal endocranial morphology is dominated by the wulst, these birds probably adopted the strategy of enlargement and orientation of the visual system to develop good stereoscopic vision and accurate depth perception. This would preadapt them to being specialised browsers capable of selecting individual fruit and leaves from within complex browse. Additionally, such combined features of cranial and endocranial morphology also raises the possibility that dromornithids were adaptively selected for low-light visual proficiency along the nocturnal-diurnal gradient (scotopic *sensu* [142,146]). However, we prefer the more 'parsimonious' explanation that features of dromornithid cranial and endocranial anatomy are more likely associated with foraging and locomotion within complex diurnal environments.

4.4.2.2. Cerebrum

The rostral and caudal telencephalon—the nido- and mesopallial structures of the cerebrum—are recognised to form a complex with "integrative" functions (see [93], and references therein). Thus, we describe functional interpretations for the cerebrum as a whole.

The internal structure of the dorsal and rostrocaudolateral cerebrum incorporates four main subdivisions: the hyperpallium, incorporating the wulst, the mesopallium, incorporating the rostro- and caudodorsal telencephalon, the nidopallium, incorporating the rostro- and caudolateral telencephalon, and the arcopallium incorporating the caudoventral telencephalon. The rostromediolateral telencephalon incorporates the medial striatopallidal complex (striatum + pallidum), overlain rostrocaudally and dorsolaterally by the nidopallium, which is similarly overlain rostrocaudally and dorsolaterally by the mesopallium (see [48] (Figure 1C), [49] (Figure 6)). Dubbeldam and Visser [147] showed that the caudolateral nidopallium receives arcopallial afferents sourced through the medial nidopallium, and contains a complex pattern of terminal fields. They identified a strong connection between the striatopallidal complex and the mediolateral nidopallium, arguing that in the mallard (*Anas platyrhynchos*) there exists two major telencephalic circuits: one relaying through the pallidum, and the other through the striatum (e.g., [48] (Figure 3)), and that these afferent circuits play a major role in feeding behaviour. The telencephalon has been associated with a wide range of behaviours including feeding, taste, tactile sense, taste discrimination, vocalisation, and with high levels of cognition and complex tasks ([49], and references therein). Furthermore, stereotyped species-specific behaviour [93,148], pecking accuracy [149], and the processing of visual information such as brightness, colour, and pattern discrimination [118], have been attributed to processes within the caudolateral telencephalon. Pettigrew and Frost [130] showed that the maxillary (V_2) division of the trigeminal (V) nerve, which innervates the upper bill (see Section 4.4.1 above), transmits to extensive terminal fields in the region of the rostrodorsal mesopallium (e.g., [150] (Figure 3b), see also [139]). Similarly, Dubbeldam et al. [99] showed that ascending maxillary (V_2) and mandibular (V_3) trigeminal (V) projections transmitted rostrodorsally, via the nucleus basalis, to mesopallial terminal fields [140]. These sensorimotor and somatosensory projections were related to the "detection" of food particles, particularly in low-visibility feeding in anseriforms [151–154], and food grasping in columbiforms [140,155] and passeriforms [156]. Located in the caudal telencephalon, the medial spiriform nucleus receives projections from both somatosensory and visual parts of the wulst (see [121]; and Section 4.4.2.1 above), along with arcopallial projections associated with "motor planning information" from the caudoventral telencephalon, and projects to the cerebellum (see Section 4.4.2.4 below), forming the "telencephalic–cerebellar loop" (*sensu* [150] (p. 9)).

A notable caveat when interpreting differences in caudal telencephalon morphology, is that changes may arise from differential hypertrophy of any of several internal structures, each of which vary in function (e.g., [157], and above). Results show that the caudal telencephalon in dromornithids are strongly hypertrophied, and along with the apparently hypotrophied rostral telencephalon, they are morphologically similar to galliforms in the condition of the cerebrum (see Sections 4.1.4 and 4.1.5). Extant galliforms are generally visual foragers and exploit less somatosensory information associated with trigeminal (V) projections than tactile specialists like anseriforms [152–154]. Results show surface area ratios for the face of the maxillomandibular (V_2 + V_3) branch of the trigeminal (V) nerve complex in dromornithids are more similar to those of the galliforms, than they are to the anseriforms, which are distinctly larger (see Section 3.4.1). These morphological trends suggest that the tactile capability of dromornithids was likely reasonably well developed, at least comparable with the extant galliforms, but they were certainly not tactile sensory specialists.

4.4.2.3. Optic Lobe

The optic lobe forms a crucial component of the visual pathway system. Hellmann et al. [158] (p. 395) characterised the optic lobe as a "relay station" for transmitting ascending visual output to the forebrain (see Section 4.4.2.1 above), projecting descending output to the premotor regions of the hindbrain (see Section 4.4.2.4 below), and comprise multiple "retinotopically organised, and functionally specific" cell types. So called "optic flow"

(*sensu* [159]), are retinal stimuli generated by self-motion through stationary environments (see [150,160] and references therein). Optic flow stimuli are analysed by recipient nuclei in the accessory optic system and pretectum, wherein the lentiformis mesencephali, or pretectal nucleus, responds to "moving large-field" visual stimuli and generates optokinetic response for the control of posture, eye movement stabilisation, and compensatory movement during locomotion ([117,150,160–164] and references therein), facilitated by processes within the cerebellum [87,165].

Optic lobe structures in dromornithids are somewhat hypotrophied in comparison to those of the extant galloanseres. Iwaniuk et al. [166] showed that the optic lobe of the nocturnal Night parrot (*Pezoporus occidentalis*) was relatively reduced compared with those of diurnal parrots, but orbit size did not differ between them. As noted above (see Section 4.4.2.1), eye shape, corneal diameter and retinal topography are better predictors low-light sensitivity than eye size alone (e.g., [86,141,142]). What is more, Kay and Kirk [167] (p. 238) showed variation in 'retinal summation', or the ratio of photoreceptor cells in the eye which interact with a single ganglion cell in the optic (II) nerve, is indicative of the level of visual sensitivity, acuity, and photic activity. This implies that large eye size, accompanied by small optic nerve size, is indicative of nocturnal habitus.

These forms of data are often not accessible from fossil material, and as we have shown, there is much variation in overall optic lobe size across known diurnal species of galloanseres assessed here. This implies that without corroborating evidence of eye structure and optic nerve absolute size, the size of the optic lobe alone is likely not a reliable proxy for inferring photic activity for fossil taxa.

Given that optic lobe structures are primarily relay stations, their absolute size is not definitively correlated with either nocturnal or diurnal behaviour (see also [168]) although this can resolved to an extent by comparisons of orbit and foramen opticum measurements. That dromornithids have large, forward facing eyes (see Section 4.4.2.1), robust optic nerves (see Section 3.1.2), and enlarged morphology of trigeminal (V) innervation (see Section 4.4.1), further supports our argument that dromornithids were likely diurnal taxa with a strong reliance on stereopsis and trigeminal (V) somatosensory input. These results also suggest that caution is required when deriving functional or behavioural inference from comparisons of optic lobe absolute size, without accounting for the collective morphology of somatosensory "circuits" (e.g., [150] (p. 9)), such as those of the thalamofugal, tectofugal and third visual pathways (see Section 4.4.2).

4.4.2.4. Hindbrain

The cerebellum has long been associated with motor integration and posture control in birds [87]. Visual signals are projected through the third visual pathway, via the retinal-recipient nuclei of the optic lobe, to the cerebellum [87,117,165,169–171], where they facilitate obstacle avoidance responses. Additionally, Pakan and Wylie [165] suggested that folia VI–VIII of the cerebellum may be involved in "steering" functions, and Iwaniuk et al. [172] showed that VI and VII folia are hypertrophied in birds they classified as "strong fliers", and showed some evidence to support correlation of hypertrophy of the cerebellum rostral lobe with "strong hindlimbs" in birds. Additionally, due to the dura mater, or dural envelope, which encloses the brain in life, a surface endocast derived from the internal osseous endocranial capsule, may not entirely reflect actual brain morphology, although this is much less of a problem in birds than in other archosaurids (e.g., [71,173] (p. 263), [74] (p. 61)). This is apparent in the lack of folia definition in dromornithid cerebellum morphology presented here, but which was almost certainly present in life. Additionally, it is recognised that an endocast can only capture surface structures of the brain, and that where a brain region is partially occluded by another structure, the endocast will underestimate total size of that region. This is the case for the cerebellum where it is occluded rostrally by the cerebrum. Thus, analyses of the cerebellum only relate to exposed parts of this region, but we consider these were analogous between compared taxa. Therefore in our analyses, the overall shape of the exposed dromornithid cerebellum is captured, and the

broad metrics we use to describe the cerebellum illustrate well the differences in dorsal hindbrain shape across specimens.

Results for the dromornithid hindbrain, show the shapes described by the dromornithid metencephalon (cerebellum and rhombencephalon), are certainly distinct from those of the extant galloanseres. Measurement data show that the dromornithid cerebellum and rhombencephalon differ from the extant galloanseres in both length and width ratios. However, results for Surface Area data show the dromornithids overlap with the extant galloanseres in metencephalon surface area ratios. So the dromornithid hindbrain is not particularly dissimilar in overall size to those of the extant taxa, and apparent visual differences between caudal endocasts across specimens may lie in the particularly distinct hypertrophy of the dromornithid forebrain, several ratios of which certainly do differ from those of the extant galloanseres (e.g., Section 4.1.3 above). Additionally, the trend for hypertrophy of the rostrodorsal cerebellum noted in both middle Miocene dromornithid taxa, compared to that of the late Oligocene species (e.g., Section 3.3.3), may represent selection for enhanced neural capability with respect to hindlimb sensorimotor processes, facilitated within the cerebellum rostral lobe [172], as overall body size in dromornithids increased from the late Oligocene through the middle Miocene. Such morphological trends suggest that dromornithids likely maintained the capacity for capable locomotion through complex environments associated with third visual pathway processes in the hindbrain, at least comparable with the extant galliforms assessed here.

5. Conclusions

In this study, we comprehensively described dromornithid endocranial morphology for the first time, comparing endocasts for three species of *Dromornis* and *Ilbandornis woodburnei* to those of four species of extant basal galloanseres spanning the galliform–anseriform dichotomy. We compared endocasts of the Oligo–Miocene *Dromornis murrayi*, the middle Miocene *D. planei*, and the late Miocene *D. stirtoni*, to describe endocranial changes associated with neurocranial foreshortening in a temporal series along the *Dromornis* lineage. The endocasts of species of *Dromornis* were compared to that of the middle Miocene *Ilbandornis woodburnei*, revealing minimally five morphological differences between *Ilbandornis* and *Dromornis* (e.g., relating to the medial boundaries of the wulst in the rostrocaudal fissura interhemispherica zone; the caudoventral regions of the caudal telencephalon; the morphology of the rostrodorsal and caudodorsal cerebellum; and the morphology of the ventral cerebellum + pons hindbrain complex), collectively supporting the two-lineage hypothesis. Overall, dromornithid brains display morphology supporting hypotheses that they are more closely related to basal galliforms than anseriforms, in that the rostral positioning of the wulst on the dorsal endocast; the form of the maxillomandibular (V_2 + V_3), glossopharyngeal (IX) and vagus (X) nerves, and the morphology of trigeminal ganglia, are more similar to the species of galliforms assessed. Functional interpretations suggest that dromornithids were specialised herbivores that likely possessed well-developed stereoscopic depth perception and targeted a soft browse trophic niche.

The retention of a relatively large cerebellum and associated hindbrain morphology in dromornithids, such as those shown by the volant galloanseres assessed, raises the question as to why dromornithids maintained the capacity for capable movement through complex environments (see above). That these functional attributes were selected for during early dromornithid evolution is a possibility.

During the transition from the early Cenozoic through the Eocene, Australia was blanketed by predominantly warm to cool-temperate rainforest, which began to open into sclerophyllous vegetation on higher ground only during the Oligocene (see [174]). These forests became progressively drier during the transition from the Oligocene through the late Miocene, eventuating in the establishment of sclerophyllous fire-sensitive woodlands as the dominant continental floras during the Miocene ([1], see also [175]). Dromornithid evolution has a long history, and the key characteristics of the dromornithid brain were likely assembled when they first evolved into large flightless birds sometime during the

Palaeogene. During those times, dromornithids would have occupied highly complex forested environments, where the capacity for acute stereoscopic vision, the taxon's trophic preferences established, and the capability for navigating complex environments were maintained from their flighted ancestors. Dromornithids likely co-opted these traits in adapting to and exploiting the steadily drying Australian environment through their known temporal range, traits that persisted in the last dromornithid taxon of the late Pleistocene.

During the middle Miocene through to the late Pleistocene, dromornithids were likely increasingly restricted to riparian zones, or sclerophyllous woodland remnants proximal to water courses or temporary water bodies. Dromornithid fossils from these times are almost exclusively recovered from deposits derived from ancient water courses or shallow lakes. For example, their bones are relatively abundant in the fluviatile deposits of Bullock Creek LF, and Alcoota LF in the Northern Territory (see Section 1); and are common in several lacustrine sites around Lake Callabonna in the Eyre basin of Southern Australia, where dromornithid bones are found within the clays of ancient lake margins wherein birds were mired, evidently while in search of water during dry periods (e.g., [176] (p. 208), [15] (p. 3)). Consequently, from the late Miocene in particular, dromornithids may have become increasingly 'tethered' to constricting sclerophyllous woodland remnants in a drying environment, circumstances which, along with temporal overlap with newly arrived humans during the late Pleistocene [177], potentially contributed to the eventual extinction of the group.

The cranial and endocranial morphology of dromornithids is unlike any attained in the evolution of birds, and represents distinct morphological adaptations to progressively changing Australian Cenozoic environments. The specialist browsing diet of these giant birds resulted in the unique juxtaposition of large body size, deep, narrow, and elongate bills, with frontally directed eyes, affording stereoscopic vision on crania bearing minimal musculature, and like much of the idiosyncratic Australian fauna of the past, dromornithids represent combinations of unique adaptations now lost.

Supplementary Materials: The following are available online at https://www.mdpi.com/1424-2818/13/3/124/s1, Supplementary Information (SI) document [178–180], and an 'Endocasts and R code' folder, including endocasts used, R scripts and supporting data files.

Author Contributions: T.H.W. and W.D.H. designed this study, wrote and edited the manuscript. W.D.H. assembled and analysed the data. All authors have read and agreed to the published version of the manuscript.

Funding: This work was supported by the Australian Research Council DE130101133, and DP180101913 (T.H.W), and an Australian Government Research Training Program Scholarship (W.D.H).

Institutional Review Board Statement: Not applicable.

Informed Consent Statement: Not applicable.

Data Availability Statement: All primary data generated in this study are available in SI and Table 1 above. Image-stack CT data are available on request, see ReadMe.txt file (SI).

Acknowledgments: We thank Michael Archer and Suzanne Hand (University of NSW, Sydney), and Queensland Museum (Brisbane, Qld) for access to *Dromornis murrayi* specimens (QM F57984, QM F57974 and QM F50412 endocast); Adam Yates (Museum of Central Australia, Alice Springs, NT) for access to the *Dromornis planei* (NTM P9464-106) specimen; The Queen Victoria Museum and Art Gallery (Launceston, Tas) for access to the *Ilbandornis woodburnei* (QVM:2000:GFV:20) specimen. Museums Victoria (Melbourne, Vic) enabled access to the *Anhima cornuta* (MV B12574) specimen. We thank Philippa Horton and Maya Penck (South Australian Museum, Adelaide, SA) for access to *Gallus gallus* (SAM B34041), *Leipoa ocellata* (SAM B11482), and *Anseranas semipalmata* (SAM B48035) specimens. Adelaide Microscopy (University of Adelaide, SA) enabled access to the Skyscan μCT instrument. We thank Joseph Bevitt (ANSTO, Sydney, NSW) for neutron scanning of *D. planei*, and Mishelle Korlaet (SAHMRI, Adelaide, SA) for CT scanning of *D. stirtoni*, *D. murrayi* and *I. woodburnei* specimens. W.D.H thanks Gavin Prideaux, Stig Walsh, Em Sherratt, and two anonymous reviewers for their comments which substantially improved earlier versions of this manuscript.

Conflicts of Interest: The authors declare no conflict of interest.

References

1. Vickers-Rich, P. The Mesozoic and Tertiary History of Birds on the Australian Plate. In *Vertebrate Palaeontology of Australasia*; Vickers-Rich, P., Monaghan, J.M., Baird, R.F., Rich, T.H., Eds.; Pioneer Design Studios and Monash University Publications Committee: Melbourne, Australia, 1991; pp. 721–808.
2. Murray, P.F.; Vickers-Rich, P. *Magnificent Mihirungs: The Colossal Flightless Birds of the Australian Dreamtime*; Indiana University Press: Bloomington, IN, USA, 2004; p. 410.
3. Murray, P.F.; Megirian, D. The skull of dromornithid birds: Anatomical evidence for their relationship to Anseriformes. *Rec. South Aust. Mus.* **1998**, *31*, 51–97.
4. Murray, P.F.; Megirian, D. The Pwerte Marnte Marnte Local Fauna: A new vertebrate assemblage of presumed Oligocene age from the Northern Territory of Australia. *Alcheringa* **2006**, *30*, 211–228. [CrossRef]
5. Boles, W.E. The Avian Fossil Record of Australia: An Overview. In *Evolution and Biogeography of Australasian Vertebrates*; Merrick, J.R., Archer, M., Hickey, G.M., Lee, M.S.Y., Eds.; Auscipub: Sydney, Australia, 2006; pp. 387–411.
6. Worthy, T.H.; Handley, W.D.; Archer, M.; Hand, S.J. The extinct flightless mihirungs (Aves, Dromornithidae): Cranial anatomy, a new species, and assessment of Oligo-Miocene lineage diversity. *J. Vertebr. Paleontol.* **2016**, *36*, e1031345. [CrossRef]
7. Vickers-Rich, P.; Molnar, R.E. The foot of a bird from the Eocene Redbank Plains Formation of Queensland, Australia. *Alcheringa* **1996**, *20*, 21–29. [CrossRef]
8. Mayr, G. *Paleogene Fossil Birds*; Springer: Berlin, Germany, 2009; p. 262.
9. Saltré, F.; Rodríguez-Rey, M.; Brook, B.W.; Johnson, C.N.; Turney, C.S.; Alroy, J.; Cooper, A.; Beeton, N.; Bird, M.I.; Fordham, D.A. Climate change not to blame for late Quaternary megafauna extinctions in Australia. *Nat. Commun.* **2016**, *7*, 10511. [CrossRef] [PubMed]
10. Owen, R. [Part 19 of Owen's memoir on *Dinornis*, read June 4, 1872]. *P. Zool. Soc. Lond.* **1872**, *1872*, 682–683.
11. Rich, P.V. The Dromornithidae, an extinct family of large ground birds endemic to Australia. *Bur. Nat. Resour. Geol. Geophys. Bull.* **1979**, *184*, 1–194.
12. Nguyen, J.M.T.; Boles, W.E.; Hand, S.J. New material of *Barawertornis tedfordi*, a dromornithid bird from the Oligo-Miocene of Australia, and its phylogenetic implications. *Rec. Aust. Mus.* **2010**, *62*, 45–60. [CrossRef]
13. Worthy, T.H.; Yates, A. Connecting the thigh and foot: Resolving the association of post-cranial elements in the species of *Ilbandornis* (Aves: Dromornithidae). *Alcheringa* **2015**, *39*, 1–21. [CrossRef]
14. Stirling, E.C.; Zietz, A.H.C. Preliminary notes on *Genyornis newtoni*: A new genus and species of fossil struthious bird found at Lake Callabonna, South Australia. *T. Roy. Soc. South Aust.* **1896**, *20*, 171–211.
15. Wells, R.T.; Tedford, R.H. *Sthenurus* (Macropodidae: Marsupialia) from the Pleistocene of Lake Callabonna, South Australia. *B. Am. Mus. Nat. Hist.* **1995**, *225*, 3–111.
16. Stirling, E.C.; Zietz, A.H.C. *Genyornis newtoni*—A fossil struthious bird from Lake Callabonna, South Australia: Description of the bones of the leg and foot. *T. Roy. Soc. South Aust.* **1896**, *20*, 191–211.
17. Wetmore, A. A classification for the birds of the world. *Smithson. Misc. Collect.* **1960**, *139*, 1–37.
18. Rich, P.V. Changing continental arrangements and the origin of Australia's non-passeriform continental avifauna. *Emu Austral Ornithol.* **1975**, *75*, 97–112. [CrossRef]
19. Worthy, T.H.; Holdaway, R.N. *The Lost World of the Moa: Prehistoric Life of New Zealand*; Indiana University Press: Bloomington, IA, USA, 2002; p. 760.
20. Phillips, M.J.; Gibb, G.C.; Crimp, E.A.; Penny, D. Tinamous and moa flock together: Mitochondrial genome sequence analysis reveals independent losses of flight among ratites. *Syst. Biol.* **2010**, *59*, 90–107. [CrossRef]
21. Olson, S.L. The Fossil Record of Birds. In *Avian Biology*; Farner, D.S., King, J.R., Parkes, K.C., Eds.; Academic Press: New York, NY, USA, 1985; Volume 8, pp. 79–238.

22. Mayr, G. Cenozoic mystery birds–on the phylogenetic affinities of bony-toothed birds (Pelagornithidae). *Zool. Scr.* **2011**, *40*, 448–467. [CrossRef]
23. Worthy, T.H.; Mitri, M.; Handley, W.D.; Lee, M.S.Y.; Anderson, A.; Sand, C. Osteology supports a stem-Galliform affinity for the giant extinct flightless bird *Sylviornis neocaledoniae* (Sylviornithidae, Galloanseres). *PLoS ONE* **2016**, *11*, e0150871. [CrossRef]
24. Worthy, T.H.; Degrange, F.J.; Handley, W.D.; Lee, M.S.Y. The evolution of giant flightless birds and novel phylogenetic relationships for extinct fowl (Aves, Galloanseres). *Roy. Soc. Open Sci.* **2017**, *4*, 170975. [CrossRef]
25. Worthy, T.H.; Degrange, F.J.; Handley, W.D.; Lee, M.S.Y. Correction to 'The evolution of giant flightless birds and novel phylogenetic relationships for extinct fowl (Aves, Galloanseres)'. *Roy. Soc. Open Sci.* **2017**, *4*, 171621. [CrossRef] [PubMed]
26. Andors, A.V. Reappraisal of the Eocene groundbird *Diatryma* (Aves: Anserimorphae). *Nat. Hist. Mus. Los Angeles County Sci. Ser.* **1992**, *36*, 109–125.
27. Angst, D.; Lécuyer, C.; Amiot, R.; Buffetaut, E.; Fourel, F.; Martineau, F.; Legendre, S.; Abourachid, A.; Herrel, A. Isotopic and anatomical evidence of an herbivorous diet in the Early Tertiary giant bird *Gastornis*. Implications for the structure of Paleocene terrestrial ecosystems. *Naturwissenschaften* **2014**, *101*, 313–322. [CrossRef]
28. Archer, M.; Godthelp, H.; Hand, S.J.; Attenborough, D. *Australia's Lost World: Riversleigh, World Heritage Site*; New Holland Publishers: Sydney, Austrilia, 1991; p. 264.
29. Woodburne, M.O. The Alcoota Fauna, central Australia: An integrated palaeontological and geological study. *B. Bur. Min. Res. Geol. Geophy.* **1967**, *87*, 1–187.
30. Murray, P.F.; Megirian, D. Continuity and contrast in middle and late Miocene vertebrate communities from the Northern Territory. *Rec. Mus. Art Gall. Northern Terr.* **1992**, *9*, 195–218.
31. Handley, W.D.; Chinsamy, A.; Yates, A.M.; Worthy, T.H. Sexual dimorphism in the late Miocene mihirung *Dromornis stirtoni* (Aves: Dromornithidae) from the Alcoota Local Fauna of central Australia. *J. Vertebr. Paleontol.* **2016**, *36*, e1180298. [CrossRef]
32. Grellet-Tinner, G.; Spooner, N.A.; Handley, W.D.; Worthy, T.H. The *Genyornis* egg: Response to Miller et al.'s commentary on Grellet-Tinner et al., 2016. *Quaternary Sci. Rev.* **2017**, *161*, 128–133. [CrossRef]
33. Hansford, J.P.; Turvey, S.T. Unexpected diversity within the extinct elephant birds (Aves: Aepyornithidae) and a new identity for the world's largest bird. *Roy. Soc. Open Sci.* **2018**, *5*, 181295. [CrossRef]
34. Archer, M.; Godthelp, H.; Hand, S.J.; Megirian, D. Fossil mammals of Riversleigh, northwestern Queensland: Preliminary overview of biostratigraphy, correlation and environmental change. *Austr. Zool.* **1989**, *25*, 29–65. [CrossRef]
35. Archer, M.; Hand, S.J.; Godthelp, H.; Creaser, P. Correlation of the Cainozoic sediments of the Riversleigh World Heritage fossil property, Queensland, Australia. In Actes du Congrès BiochroM '97. *Mémoires Travaux Inst. Montp.* **1997**, *21*, 131–152.
36. Travouillon, K.J.; Archer, M.; Hand, S.J.; Godthelp, H. Multivariate analyses of Cenozoic mammalian faunas from Riversleigh, northwestern Queensland. *Alcheringa Spec. Iss.* **2006**, *1*, 323–349. [CrossRef]
37. Travouillon, K.J.; Escarguel, G.; Legendre, S.; Archer, M.; Hand, S.J. The use of MSR (Minimum Sample Richness) for sample assemblage comparisons. *Paleobiology* **2011**, *37*, 696–709. [CrossRef]
38. Woodhead, J.; Hand, S.J.; Archer, M.; Graham, I.; Sniderman, K.; Arena, D.A.; Black, K.H.; Godthelp, H.; Creaser, P.; Price, E. Developing a radiometrically-dated chronologic sequence for Neogene biotic change in Australia, from the Riversleigh World Heritage Area of Queensland. *Gondwana Res.* **2016**, *29*, 153–167. [CrossRef]
39. Arena, D.A.; Travouillon, K.J.; Beck, R.M.D.; Black, K.H.; Gillespie, A.K.; Myers, T.J.; Archer, M.; Hand, S.J. Mammalian lineages and the biostratigraphy and biochronology of Cenozoic faunas from the Riversleigh World Heritage Area, Australia. *Lethaia* **2016**, *49*, 43–60. [CrossRef]
40. Megirian, D.; Prideaux, G.J.; Murray, P.F.; Smit, N. An Australian land mammal age biochronological scheme. *Paleobiology* **2010**, *36*, 658–671. [CrossRef]
41. Murray, P.; Megirian, D.; Rich, T.; Plane, M.; Black, K.; Archer, M.; Hand, S.J.; Vickers-Rich, P. Morphology, systematics, and evolution of the marsupial genus *Neohelos* Stirton (Diprotodontidae, Zygomaturinae). *Mus. Gall. Northern Terr. Res. Rep.* **2000**, *6*, 1–141.
42. Yates, A.M. New craniodental remains of *Wakaleo alcootaensis* (Diprotodontia: Thylacoleonidae) a carnivorous marsupial from the late Miocene Alcoota Local Fauna of the Northern Territory, Australia. *PeerJ* **2015**, *3*, e1408. [CrossRef]
43. Yates, A.M. A new species of long-necked turtle (Pleurodira: Chelidae: *Chelodina*) from the late Miocene Alcoota Local Fauna, Northern Territory, Australia. *PeerJ* **2013**, *1*, e170. [CrossRef]
44. Worthy, T.H.; Yates, A. A review of the smaller birds from the late Miocene Alcoota Local Faunas of Australia with a description of a new species. In Proceedings of the 9th International Meeting of the Society of Avian Paleontology and Evolution, Diamante, Argentina, 1–6 August 2016. *Contr. Mus. Arg. Cien. Nat.* **2017**, *7*, 221–252.
45. Yates, A.M.; Worthy, T.H. A diminutive species of emu (Casuariidae: Dromaiinae) from the late Miocene of the Northern Territory, Australia. *J. Vertebr. Paleontol.* **2019**, *39*, e1665057. [CrossRef]
46. Stirton, R.A.; Woodburne, M.O.; Plane, M.D. A phylogeny of the Tertiary Diprotodontidae and its significance in correlation. In Tertiary Diprotodontidae from Australia and New Guinea. *B. Bur. Min. Res. Geol. Geophy.* **1967**, *85*, 149–160.
47. Baumel, J.J.; King, A.S.; Breazile, J.E.; Evans, H.E.; Vanden Berge, J.C. *Handbook of Avian Anatomy: Nomina Anatomica Avium*, 2nd ed.; Nuttall Ornithological Club: Cambridge, MA, USA, 1993; Volume 23, p. 779.
48. Jarvis, E.D.; Güntürkün, O.; Bruce, L.; Csillag, A.; Karten, H.; Kuenzel, W.; Medina, L.; Paxinos, G.; Perkel, D.J.; Shimizu, T. Avian brains and a new understanding of vertebrate brain evolution. *Nat. Rev. Neurosci.* **2005**, *6*, 151–159. [CrossRef] [PubMed]

49. Corfield, J.R.; Wild, J.M.; Parsons, S.; Kubke, M.F. Morphometric analysis of telencephalic structure in a variety of neognath and paleognath bird species reveals regional differences associated with specific behavioral traits. *Brain Behav. Evolut.* **2012**, *80*, 181–195. [CrossRef] [PubMed]
50. Early, C.M.; Iwaniuk, A.N.; Ridgely, R.C.; Witmer, L.M. Endocast structures are reliable proxies for the sizes of corresponding regions of the brain in extant birds. *J. Anat.* **2020**, *237*, 1162–1176. [CrossRef]
51. Rasband, W.S. *ImageJ*; U.S. National Institute of Health: Bethesda, MD, USA, 2018. Available online: https://imagej.nih.gov/ij/ (accessed on 28 January 2021).
52. Cignoni, P.; Callieri, M.; Corsini, M.; Dellepiane, M.; Ganovelli, F.; Ranzuglia, G. Year Meshlab: An open-source mesh processing tool. In *Eurographics Italian Chapter Conference*; Scarano, V., De Chiara, R., Erra, U., Eds.; The Eurographics Association: Geneve, Switzerland, 2008; pp. 129–136. [CrossRef]
53. Wiley, D.F. *Landmark Editor 3.0*; Institute for Data Analysis and Visualization, University of California: Davis, CA, USA, 2006.
54. Bookstein, F.L. *Morphometric Tools for Landmark Data: Geometry and Biology*; Cambridge University Press: Cambridge, UK, 1991; p. 435.
55. Adams, D.C.; Collyer, M.L.; Kaliontzopoulou, A. Geomorph: Software for Geometric Morphometric Analyses. R Package Version 3.1.0. 2019. Available online: https://cran.r-project.org/src/contrib/Archive/geomorph/ (accessed on 25 March 2019).
56. Mosimann, J.E. Size allometry: Size and shape variables with characterizations of the lognormal and generalized gamma distributions. *J. Am. Stat. Assoc.* **1970**, *65*, 930–945. [CrossRef]
57. Claude, J. *Morphometrics with R*; Springer: New York, NY, USA, 2008; p. 316.
58. Klingenberg, C.P. Size, shape, and form: Concepts of allometry in geometric morphometrics. *Dev. Genes Evol.* **2016**, *226*, 113–137. [CrossRef] [PubMed]
59. Sherratt, E.; Vidal-García, M.; Anstis, M.; Keogh, J.S. Adult frogs and tadpoles have different macroevolutionary patterns across the Australian continent. *Nat. Ecol. Evol.* **2017**, *1*, 1385–1391. [CrossRef] [PubMed]
60. R Core Team. *R: A Language and Environment for Statistical Computing*; R Foundation for Statistical Computing: Vienna, Austria, 2019; Available online: https://www.R-project.org/ (accessed on 28 January 2021).
61. RStudio Team. *RStudio: Integrated Development for R*; RStudio, Inc.: Boston, MA, USA, 2019; Available online: http://www.rstudio.com/ (accessed on 28 January 2021).
62. Gower, J.C. Generalized Procrustes analysis. *Psychometrika* **1975**, *40*, 33–51. [CrossRef]
63. Rohlf, F.J.; Slice, D. Extensions of the Procrustes method for the optimal superimposition of landmarks. *Syst. Biol.* **1990**, *39*, 40–59. [CrossRef]
64. Bookstein, F.L. Size and shape spaces for landmark data in two dimensions. *Stat. Sci.* **1986**, *1*, 181–242. [CrossRef]
65. Adams, D.C.; Otárola-Castillo, E. geomorph: An R package for the collection and analysis of geometric morphometric shape data. *Methods Ecol. Evol.* **2013**, *4*, 393–399. [CrossRef]
66. Bookstein, F.L. Landmark methods for forms without landmarks: Morphometrics of group differences in outline shape. *Med. Image Anal.* **1997**, *1*, 225–243. [CrossRef]
67. Bookstein, F.L. Shape and the information in medical images: A decade of the morphometric synthesis. *Comput. Vis. Image Und.* **1997**, *2*, 97–118. [CrossRef]
68. Iwaniuk, A.N.; Nelson, J.E. Can endocranial volume be used as an estimate of brain size in birds? *Can. J. Zool.* **2002**, *80*, 16–23. [CrossRef]
69. Striedter, G.F. *Principles of Brain Evolution*; Sinauer Associates: Sunderland, MA, USA, 2005.
70. Striedter, G.F. Précis of principles of brain evolution. *Behav. Brain Sci.* **2006**, *29*, 1–12. [CrossRef]
71. Witmer, L.M.; Ridgely, R.C.; Dufeau, D.L.; Semones, M.C. Using CT to Peer into the Past: 3D Visualization of the Brain and Ear Regions of Birds, Crocodiles, and Nonavian Dinosaurs. In *Anatomical Imaging, Towards a New Morphology*; Endo, H., Frey, R., Eds.; Springer: Tokyo, Japan, 2008; pp. 67–87.
72. Picasso, M.B.J.; Tambussi, C.; Dozo, M.T. Neurocranial and brain anatomy of a Late Miocene eagle (Aves, Accipitridae) from Patagonia. *J. Vertebr. Paleontol.* **2009**, *29*, 831–836. [CrossRef]
73. Walsh, S.A.; Iwaniuk, A.N.; Knoll, M.A.; Bourdon, E.; Barrett, P.M.; Milner, A.C.; Nudds, R.L.; Abel, R.L.; Sterpaio, P.D. Avian cerebellar floccular fossa size is not a proxy for flying ability in birds. *PLoS ONE* **2013**, *8*, e67176. [CrossRef] [PubMed]
74. Walsh, S.A.; Knoll, F. The Evolution of Avian Intelligence and Sensory Capabilities: The Fossil Evidence. In *Digital Endocasts: From Skulls to Brains*; Bruner, E., Ogihara, N., Tanabe, H.C., Eds.; Springer: Tokyo, Japan, 2018; pp. 59–69.
75. Scofield, R.P.; Ashwell, K.W.S. Rapid somatic expansion causes the brain to lag behind: The case of the brain and behavior of New Zealand's Haast's Eagle (*Harpagornis moorei*). *J. Vertebr. Paleontol.* **2009**, *29*, 637–649. [CrossRef]
76. Lawal, R.A.; Al-Atiyat, R.M.; Aljumaah, R.S.; Silva, P.; Mwacharo, J.M.; Hanotte, O. Whole-genome resequencing of red junglefowl and indigenous village chicken reveal new insights on the genome dynamics of the species. *Front. Genet.* **2018**, *9*, 264. [CrossRef] [PubMed]
77. Ashwell, K.W.S.; Scofield, R.P. Big birds and their brains: Paleoneurology of the New Zealand moa. *Brain Behav. Evolut.* **2008**, *71*, 151–166. [CrossRef] [PubMed]
78. Craigie, E.H. The cerebral cortex of *Rhea americana*. *J. Comp. Neurol.* **1939**, *70*, 331–353. [CrossRef]
79. Martin, G.R.; Wilson, K.-J.; Wild, J.M.; Parsons, S.; Kubke, M.F.; Corfield, J. Kiwi forego vision in the guidance of their nocturnal activities. *PLoS ONE* **2007**, *2*, e198. [CrossRef]

80. Peng, K.; Feng, Y.; Zhang, G.; Liu, H.; Song, H. Anatomical study of the brain of the African ostrich. *Turk. J. Vet. Anim. Sci.* **2010**, *34*, 235–241. [CrossRef]
81. Picasso, M.B.J.; Tambussi, C.P.; Degrange, F.J. Virtual reconstructions of the endocranial cavity of *Rhea americana* (Aves, Palaeognathae): Postnatal anatomical changes. *Brain Behav. Evolut.* **2011**, *76*, 176–184. [CrossRef] [PubMed]
82. Witmer, L.M.; Chatterjee, S.; Franzosa, J.; Rowe, T. Neuroanatomy of flying reptiles and implications for flight, posture and behaviour. *Nature* **2003**, *425*, 950–953. [CrossRef]
83. Milner, A.C.; Walsh, S.A. Avian brain evolution: New data from Palaeogene birds (Lower Eocene) from England. *Zool. J. Linn. Soc. Lond.* **2009**, *155*, 198–219. [CrossRef]
84. Witmer, L.M.; Ridgely, R.C. New insights into the brain, braincase, and ear region of tyrannosaurs (Dinosauria, Theropoda), with implications for sensory organization and behavior. *Anat. Rec.* **2009**, *292*, 1266–1296. [CrossRef]
85. Walsh, S.A.; Luo, Z.-X.; Barrett, P.M. Modern Imaging Techniques as a Window to Prehistoric Auditory Worlds. In *Insights from Comparative Hearing Research*; Koppl, C., Manley, G.A., Popper, A.N., Fay, R.R., Eds.; Springer: New York, NY, USA, 2014; pp. 227–261.
86. Hall, M.I.; Iwaniuk, A.N.; Gutiérrez-Ibáñez, C. Optic foramen morphology and activity pattern in birds. *Anat. Rec.* **2009**, *292*, 1827–1845. [CrossRef]
87. Jerison, H.J. *Evolution of the Brain and Intelligence*; Academic Press: New York, NY, USA, 1973; p. 482.
88. Barton, R.A.; Purvis, A.; Harvey, P.H. Evolutionary radiation of visual and olfactory brain systems in primates, bats and insectivores. *Philos. T. Roy. Soc. B.* **1995**, *348*, 381–392.
89. Barton, R.A.; Aggleton, J.P.; Grenyer, R. Evolutionary coherence of the mammalian amygdala. *P. Roy. Soc. B. Biol. Sci.* **2003**, *270*, 539–543. [CrossRef]
90. Barton, R.A.; Harvey, P.H. Mosaic evolution of brain structure in mammals. *Nature* **2000**, *405*, 1055–1058. [CrossRef] [PubMed]
91. Whiting, B.A.; Barton, R.A. The evolution of the cortico-cerebellar complex in primates: Anatomical connections predict patterns of correlated evolution. *J. Hum. Evolut.* **2003**, *44*, 3–10. [CrossRef]
92. Iwaniuk, A.N.; Dean, K.M.; Nelson, J.E. A mosaic pattern characterizes the evolution of the avian brain. *P. Roy. Soc. B. Biol. Sci.* **2004**, *271*, S148–S151. [CrossRef] [PubMed]
93. Dubbeldam, J.L. Birds. In *The Central Nervous System of Vertebrates*; Nieuwenhuys, R., ten Donkelaar, H.J., Nicholson, C., Eds.; Springer: Berlin, Germany, 1998; pp. 1525–1636.
94. Iwaniuk, A.N.; Heesy, C.P.; Hall, M.I.; Wylie, D.R. Relative wulst volume is correlated with orbit orientation and binocular visual field in birds. *J. Comp. Physiol. A.* **2008**, *194*, 267–282. [CrossRef]
95. Corfield, J.R.; Price, K.; Iwaniuk, A.N.; Gutiérrez-Ibáñez, C.; Birkhead, T.; Wylie, D.R. Diversity in olfactory bulb size in birds reflects allometry, ecology, and phylogeny. *Front. Neuroanat.* **2015**, *9*, 102. [CrossRef] [PubMed]
96. Gutiérrez-Ibáñez, C.; Iwaniuk, A.N.; Wylie, D.R. The independent evolution of the enlargement of the principal sensory nucleus of the trigeminal nerve in three different groups of birds. *Brain Behav. Evolut.* **2009**, *74*, 280–294. [CrossRef] [PubMed]
97. Dubbeldam, J.L. Studies on the somatotopy of the trigeminal system in the mallard, *Anas platyrhynchos L.* II. Morphology of the principal sensory nucleus. *J. Comp. Neurol.* **1980**, *191*, 557–571. [CrossRef]
98. Bubień-Waluszewska, A. The Cranial Nerves. In *Form and Function in Birds*; King, A.S., McLelland, J., Eds.; Academic Press: London, UK, 1981; Volume 2, pp. 385–438.
99. Dubbeldam, J.L.; Brauch, C.S.M.; Don, A. Studies on the somatotopy of the trigeminal system in the mallard, *Anas platyrhynchos L.* III. Afferents and organization of the nucleus basalis. *J. Comp. Neurol.* **1981**, *196*, 391–405. [CrossRef]
100. Wild, J.M.; Zeigler, H.P. Central projections and somatotopic organisation of trigeminal primary afferents in pigeon (*Columba livia*). *J. Comp. Neurol.* **1996**, *368*, 136–152. [CrossRef]
101. Dubbeldam, J.L.; Brus, E.R.; Menken, S.B.J.; Zeilstra, S. The central projections of the glossopharyngeal and vagus ganglia in the mallard, *Anas platyrhynchos* L. *J. Comp. Neurol.* **1979**, *183*, 149–168. [CrossRef]
102. Wild, J.M.; Zeigler, H.P. Central representation and somatotopic organization of the jaw muscles within the facial and trigeminal nuclei of the pigeon (*Columba livia*). *J. Comp. Neurol.* **1980**, *192*, 175–201. [CrossRef]
103. Wild, J.M. Identification and localization of the motor nuclei and sensory projections of the glossopharyngeal, vagus, and hypoglossal nerves of the cockatoo (*Cacatua roseicapilla*), Cacatuidae. *J. Comp. Neurol.* **1981**, *203*, 351–377. [CrossRef]
104. Wild, J.M. Peripheral and central terminations of hypoglossal afferents innervating lingual tactile mechanoreceptor complexes in Fringillidae. *J. Comp. Neurol.* **1990**, *298*, 157–171. [CrossRef] [PubMed]
105. Dubbeldam, J.L. The sensory trigeminal system in birds: Input, organization and effects of peripheral damage. *Arch. Physiol. Biochem.* **1998**, *106*, 338–345. [CrossRef]
106. Wild, J.M. The avian somatosensory system: Connections of regions of body representation in the forebrain of the pigeon. *Brain Res.* **1987**, *412*, 205–223. [CrossRef]
107. Dubbeldam, J.L. Cranial nerves and sensory centres—A matter of definition? Hypoglossal and other afferents of the avian sensory trigeminal system. *Zool. Jahrb.* **1992**, *122*, 179–186.
108. Dubbeldam, J.L. Afferent connections of nervus facialis and nervus glossopharyngeus in the pigeon (*Columba livia*) and their role in feeding behavior. *Brain Behav. Evolut.* **1984**, *24*, 47–57. [CrossRef] [PubMed]
109. Arends, J.J.A.; Dubbeldam, J.L. The subnuclei and primary afferents of the descending trigeminal system in the mallard (*Anas platyrhynchos L.*). *Neuroscience* **1984**, *13*, 781–795. [CrossRef]

110. Davies, S.J.J.F. The food of emus. *Austral Ecol.* **1978**, *3*, 411–422. [CrossRef]
111. Davies, S.J.J.F. *Bird Families of the World: Ratites and Tinamous: Tinamidae, Rheidae, Dromaiidae, Casuariidae, Apterygidae, Struthionidae*; Oxford University Press: Oxford, UK, 2002; p. 310.
112. Wings, O. A review of gastrolith function with implications for fossil vertebrates and a revised classification. *Acta Palaeontol. Pol.* **2007**, *52*, 1–16.
113. Fritz, J.; Hummel, J.; Kienzle, E.; Wings, O.; Streich, W.J.; Clauss, M. Gizzard vs. teeth, it's a tie: Food-processing efficiency in herbivorous birds and mammals and implications for dinosaur feeding strategies. *Paleobiology* **2011**, *37*, 577–586. [CrossRef]
114. Worthy, T.H. Aspects of the biology of two moa species (Aves: Dinornithiformes). *New Zeal. J. Arch.* **1989**, *11*, 77–86.
115. Wood, J.R.; Rawlence, N.J.; Rogers, G.M.; Austin, J.J.; Worthy, T.H.; Cooper, A. Coprolite deposits reveal the diet and ecology of the extinct New Zealand megaherbivore moa (Aves, Dinornithiformes). *Quat. Sci. Rev.* **2008**, *27*, 2593–2602. [CrossRef]
116. Wood, J.R.; Wilmshurst, J.M.; Richardson, S.J.; Rawlence, N.J.; Wagstaff, S.J.; Worthy, T.H.; Cooper, A. Resolving lost herbivore community structure using coprolites of four sympatric moa species (Aves: Dinornithiformes). *Pro. Natl. Acad. Sci. USA* **2013**, *110*, 16910–16915. [CrossRef]
117. Wylie, D.R.; Gutiérrez-Ibáñez, C.; Pakan, J.M.P.; Iwaniuk, A.N. The optic tectum of birds: Mapping our way to understanding visual processing. *Can. J. Exp. Psychol.* **2009**, *63*, 328–338. [CrossRef] [PubMed]
118. Iwaniuk, A.N.; Gutiérrez-Ibáñez, C.; Pakan, J.M.P.; Wylie, D.R. Allometric scaling of the tectofugal pathway in birds. *Brain Behav. Evolut.* **2010**, *75*, 122–137. [CrossRef]
119. Wylie, D.R.; Iwaniuk, A.N. Neural Mechanisms Underlying Visual Motion Detection in Birds. In *How Animals See the World: Comparative Behavior, Biology, and Evolution of Vision*; Lazareva, O.F., Shimizu, T., Wasserman, E.A., Eds.; Oxford University Press: New York, NY, USA, 2012; pp. 289–318.
120. Iwaniuk, A.N.; Wylie, D.R. The evolution of stereopsis and the wulst in caprimulgiform birds: A comparative analysis. *J. Comp. Physiol. A* **2006**, *192*, 1313–1326. [CrossRef] [PubMed]
121. Wild, J.M.; Williams, M.N. Rostral wulst in passerine birds. I. Origin, course, and terminations of an avian pyramidal tract. *J. Comp. Neurol.* **2000**, *416*, 429–450. [CrossRef]
122. Miceli, D.; Marchand, L.; Repérant, J.; Rio, J.-P. Projections of the dorsolateral anterior complex and adjacent thalamic nuclei upon the visual wulst in the pigeon. *Brain Res.* **1990**, *518*, 317–323. [CrossRef]
123. Deng, C.; Wang, B. Overlap of somatic and visual response areas in the wulst of pigeon. *Brain Res.* **1992**, *582*, 320–322.
124. Stingelin, W. *Vergleichende Morphologische Untersuchungen am Vorderhirn der Vögel auf Cytologischer und Cytoarchitektonischer Grundlage*; Verlag Helbing & Lichtenhahn: Basel, Switzerland, 1957; p. 123.
125. Pettigrew, J.D. Evolution of Binocular Vision. In *Visual Neuroscience*; Pettigrew, J.D., Sanderson, K.J., Levick, W.R., Eds.; Springer: New York, NY, USA, 1986; pp. 208–222.
126. Rogers, L. Behavioral, structural and neurochemical asymmetries in the avian brain: A model system for studying visual development and processing. *Neurosci. Biobehav. Rev.* **1996**, *20*, 487–503. [CrossRef]
127. Wild, J.M.; Kubke, M.F.; Peña, J.L. A pathway for predation in the brain of the barn owl (*Tyto alba*): Projections of the gracile nucleus to the "claw area" of the rostral wulst via the dorsal thalamus. *J. Comp. Neurol.* **2008**, *509*, 156–166. [CrossRef]
128. Wild, J.M. The avian somatosensory system: The pathway from wing to wulst in a passerine (*Chloris chloris*). *Brain Res.* **1997**, *759*, 122–134. [CrossRef]
129. Manger, P.R.; Elston, G.N.; Pettigrew, J.D. Multiple maps and activity-dependent representational plasticity in the anterior wulst of the adult barn owl (*Tyto alba*). *Eur. J. Neurosci.* **2002**, *16*, 743–750. [CrossRef] [PubMed]
130. Pettigrew, J.D.; Frost, B.J. A tactile fovea in the Scolopacidae? *Brain Behav. Evolut.* **1985**, *26*, 185–195. [CrossRef]
131. Martin, G.R. What is binocular vision for? A birds' eye view. *J. Vision.* **2009**, *9*, 1–19. [CrossRef]
132. Wylie, D.R.; Gutiérrez-Ibáñez, C.; Iwaniuk, A.N. Integrating brain, behavior, and phylogeny to understand the evolution of sensory systems in birds. *Front. Neurosci. Switz.* **2015**, *9*, 281. [CrossRef] [PubMed]
133. Pettigrew, J.D.; Konishi, M. Neurons selective for orientation and binocular disparity in the visual wulst of the barn owl (*Tyto alba*). *Science* **1976**, *193*, 675–678. [CrossRef]
134. Pettigrew, J.D. Binocular visual processing in the owl's telencephalon. *Proc. Roy. Soc. B Biol. Sci.* **1979**, *204*, 435–454. [CrossRef]
135. Van der Willigen, R.F.; Frost, B.J.; Wagner, H. Stereoscopic depth perception in the owl. *NeuroReport* **1998**, *9*, 1233–1237. [CrossRef]
136. Orlowski, J.; Harmening, W.; Wagner, H. Night vision in barn owls: Visual acuity and contrast sensitivity under dark adaptation. *J. Vision.* **2012**, *12*, 1–8. [CrossRef]
137. Gutiérrez-Ibáñez, C.; Iwaniuk, A.N.; Lisney, T.J.; Wylie, D.R. Comparative study of visual pathways in owls (Aves: Strigiformes). *Brain Behav. Evolut.* **2013**, *81*, 27–39. [CrossRef] [PubMed]
138. Kulemeyer, C.; Asbahr, K.; Gunz, P.; Frahnert, S.; Bairlein, F. Functional morphology and integration of corvid skulls–a 3D geometric morphometric approach. *Front. Zool.* **2009**, *6*, 1–14. [CrossRef] [PubMed]
139. Northcutt, R.G. Evolution of the telencephalon in nonmammals. *Annu. Rev. Neurosci.* **1981**, *4*, 301–350. [CrossRef] [PubMed]
140. Wild, J.M.; Arends, J.J.A.; Zeigler, H.P. Telencephalic connections of the trigeminal system in the pigeon (*Columba livia*): A trigeminal sensorimotor circuit. *J. Comp. Neurol.* **1985**, *234*, 441–464. [CrossRef]
141. Hall, M.I.; Ross, C.F. Eye shape and activity pattern in birds. *J. Zool.* **2007**, *271*, 437–444. [CrossRef]
142. Hall, M.I. The anatomical relationships between the avian eye, orbit and sclerotic ring: Implications for inferring activity patterns in extinct birds. *J. Anat.* **2008**, *212*, 781–794. [CrossRef] [PubMed]

143. Iwaniuk, A.N.; Heesy, C.P.; Hall, M.I. Morphometrics of the eyes and orbits of the nocturnal swallow-tailed gull (*Creagrus furcatus*). *Can. J. Zool.* **2010**, *88*, 855–865. [CrossRef]
144. Corfield, J.R.; Gsell, A.C.; Brunton, D.; Heesy, C.P.; Hall, M.I.; Acosta, M.L.; Iwaniuk, A.N. Anatomical specializations for nocturnality in a critically endangered parrot, the Kakapo (*Strigops habroptilus*). *PLoS ONE* **2011**, *6*, e22945. [CrossRef]
145. Corfield, J.R.; Wild, J.M.; Hauber, M.E.; Parsons, S.; Kubke, M.F. Evolution of brain size in the palaeognath lineage, with an emphasis on New Zealand ratites. *Brain Behav. Evolut.* **2008**, *71*, 87–99. [CrossRef]
146. Garamszegi, L.Z.; Møller, A.P.; Erritzøe, J. Coevolving avian eye size and brain size in relation to prey capture and nocturnality. *Proc. Roy. Soc. B Biol. Sci.* **2002**, *269*, 961–967. [CrossRef]
147. Dubbeldam, J.L.; Visser, A.M. The organization of the nucleus basalis—neostriatum complex of the mallard (*Anas platyrhynchos L.*) and its connections with the archistriatum and the paleostriatum complex. *Neuroscience* **1987**, *21*, 487–517. [CrossRef]
148. Reiner, A.; Davis, B.M.; Brecha, N.C.; Karten, H.J. The distribution of enkephalinlike immunoreactivity in the telencephalon of the adult and developing domestic chicken. *J. Comp. Neurol.* **1984**, *228*, 245–262. [CrossRef]
149. Salzen, E.A.; Parker, D.M.; Williamson, A.J. A forebrain lesion preventing imprinting in domestic chicks. *Exp. Brain Res.* **1975**, *24*, 145–157. [CrossRef] [PubMed]
150. Iwaniuk, A.N.; Wylie, D.R. Sensory systems in birds: What we have learned from studying sensory specialists. *J. Comp. Neurol.* **2020**, *528*, 2902–2918. [CrossRef] [PubMed]
151. Berkhoudt, H.; Dubbeldam, J.L.; Zeilstra, S. Studies on the somatotopy of the trigeminal system in the mallard, *Anas platyrhynchos L.* IV. Tactile representation in the nucleus basalis. *J. Comp. Neurol.* **1981**, *196*, 407–420. [CrossRef]
152. Schneider, E.R.; Mastrotto, M.; Laursen, W.J.; Schulz, V.P.; Goodman, J.B.; Funk, O.H.; Gallagher, P.G.; Gracheva, E.O.; Bagriantsev, S.N. Neuronal mechanism for acute mechanosensitivity in tactile-foraging waterfowl. *Pro. Natl. Acad. Sci. USA* **2014**, *111*, 14941–14946. [CrossRef] [PubMed]
153. Schneider, E.R.; Anderson, E.O.; Mastrotto, M.; Matson, J.D.; Schulz, V.P.; Gallagher, P.G.; LaMotte, R.H.; Gracheva, E.O.; Bagriantsev, S.N. Molecular basis of tactile specialization in the duck bill. *Pro. Natl. Acad. Sci. USA* **2017**, *114*, 13036–13041. [CrossRef]
154. Schneider, E.R.; Anderson, E.O.; Feketa, V.V.; Mastrotto, M.; Nikolaev, Y.A.; Gracheva, E.O.; Bagriantsev, S.N. A cross-species analysis reveals a general role for Piezo2 in mechanosensory specialization of trigeminal ganglia from tactile specialist birds. *Cell Rep.* **2019**, *26*, 1979–1987. [CrossRef]
155. Wild, J.M.; Arends, J.J.A.; Zeigler, H.P. A trigeminal sensorimotor circuit for pecking, grasping and feeding in the pigeon (*Columba livia*). *Brain Res.* **1984**, *300*, 146–151. [CrossRef]
156. Wild, J.M.; Farabaugh, S.M. Organization of afferent and efferent projections of the nucleus basalis prosencephali in a passerine, *Taeniopygia guttata*. *J. Comp. Neurol.* **1996**, *365*, 306–328. [CrossRef]
157. Von Eugen, K.; Tabrik, S.; Güntürkün, O.; Ströckens, F. A comparative analysis of the dopaminergic innervation of the executive caudal nidopallium in pigeon, chicken, zebra finch, and carrion crow. *J. Comp. Neurol.* **2020**, *528*, 2929–2955. [CrossRef]
158. Hellmann, B.; Güntürkün, O.; Manns, M. Tectal mosaic: Organization of the descending tectal projections in comparison to the ascending tectofugal pathway in the pigeon. *J. Comp. Neurol.* **2004**, *472*, 395–410. [CrossRef]
159. Gibson, J.J. The visual perception of objective motion and subjective movement. *Psychol. Rev.* **1954**, *61*, 304–314. [CrossRef] [PubMed]
160. Wylie, D.R.; Gutiérrez-Ibáñez, C.; Gaede, A.H.; Altshuler, D.L.; Iwaniuk, A.N. Visual-cerebellar pathways and their roles in the control of avian flight. *Front. Neurosci. Switz.* **2018**, *12*, 223. [CrossRef] [PubMed]
161. Simpson, J.I. The accessory optic system. *Annu. Rev. Neurosci.* **1984**, *7*, 13–41. [CrossRef]
162. Simpson, J.I.; Leonard, C.S.; Soodak, R.E. The accessory optic system. Analyzer of self-motion. *Ann. N. Y. Acad. Sci.* **1988**, *545*, 170–179. [CrossRef] [PubMed]
163. Giolli, R.A.; Blanks, R.H.; Lui, F. The accessory optic system: Basic organization with an update on connectivity, neurochemistry, and function. *Prog. Brain Res.* **2006**, *151*, 407–440.
164. Gaede, A.H.; Gutiérrez-Ibáñez, C.; Armstrong, M.S.; Altshuler, D.L.; Wylie, D.R. Pretectal projections to the oculomotor cerebellum in hummingbirds (*Calypte anna*), zebra finches (*Taeniopygia guttata*), and pigeons (*Columba livia*). *J. Comp. Neurol.* **2019**, *527*, 2644–2658. [CrossRef]
165. Pakan, J.M.P.; Wylie, D.R. Two optic flow pathways from the pretectal nucleus lentiformis mesencephali to the cerebellum in pigeons (*Columba livia*). *J. Comp. Neurol.* **2006**, *499*, 732–744. [CrossRef] [PubMed]
166. Iwaniuk, A.N.; Keirnan, A.R.; Janetzki, H.; Mardon, K.; Murphy, S.; Leseberg, N.P.; Weisbecker, V. The endocast of the Night Parrot (*Pezoporus occidentalis*) reveals insights into its sensory ecology and the evolution of nocturnality in birds. *Sci. Rep.* **2020**, *10*, 9258. [CrossRef] [PubMed]
167. Kay, R.F.; Kirk, E.C. Osteological evidence for the evolution of activity pattern and visual acuity in primates. *Am. J. Phys. Anthropol.* **2000**, *113*, 235–262. [CrossRef]
168. Bennett, P.M.; Harvey, P.H. Relative brain size and ecology in birds. *J. Zool.* **1985**, *207*, 151–169. [CrossRef]
169. Lau, K.L.; Glover, R.G.; Linkenhoker, B.; Wylie, D.R. Topographical organization of inferior olive cells projecting to translation and rotation zones in the vestibulocerebellum of pigeons. *Neuroscience* **1998**, *85*, 605–614. [CrossRef]
170. Wylie, D.R. Projections from the nucleus of the basal optic root and nucleus lentiformis mesencephali to the inferior olive in pigeons (*Columba livia*). *J. Comp. Neurol.* **2001**, *429*, 502–513. [CrossRef]

171. Wylie, D.R. Processing of visual signals related to self-motion in the cerebellum of pigeons. *Front. Behav. Neurosci.* **2013**, *7*, 1–15. [CrossRef] [PubMed]
172. Iwaniuk, A.N.; Hurd, P.L.; Wylie, D.R. Comparative morphology of the avian cerebellum: II. Size of folia. *Brain Behav. Evolut.* **2007**, *69*, 196–219. [CrossRef]
173. Walsh, S.A.; Knoll, M.A. Directions in palaeoneurology. *Spec. Pap. Palaeontol.* **2011**, *86*, 263–279. [CrossRef]
174. Martin, H.A. Cenozoic climatic change and the development of the arid vegetation in Australia. *J. Arid Environ.* **2006**, *66*, 533–563. [CrossRef]
175. Macphail, M.K. Late Neogene climates in Australia: Fossil pollen-and spore-based estimates in retrospect and prospect. *Aust. J. Bot.* **1997**, *45*, 425–464. [CrossRef]
176. Stirling, E.C. The recent discovery of fossil remains at Lake Callabonna, South Australia II. *Nature* **1894**, *50*, 206–211.
177. Hamm, G.; Mitchell, P.; Arnold, L.J.; Prideaux, G.J.; Questiaux, D.; Spooner, N.A.; Levchenko, V.A.; Foley, E.C.; Worthy, T.H.; Stephenson, B. Cultural innovation and megafauna interaction in the early settlement of arid Australia. *Nature* **2016**, *539*, 280–283. [CrossRef]
178. Szabo, M.J. Stout-legged moa. *New Zeal. Birds Online*. 2013. Available online: http://www.nzbirdsonline.org.nz (accessed on 17 April 2020).
179. Alexander, R.M. Allometry of the leg bones of moas (Dinornithes) and other birds. *J. Zool. Lond.* **1983**, *200*, 215–231. [CrossRef]
180. Campbell, K.E., Jr.; Marcus, L. The relationship of hindlimb bone dimensions to body weight in birds. *Nat. Hist. Mus. Los Angeles County Sci. Ser.* **1992**, *36*, 395–412.